



## Research Article

# Semiactive Control of Nonlinear Parametric Vibration of Super-Long Stay Cable in Cable-Stayed Bridge Installed with Magnetorheological Fluid Damper

Junping Du <sup>1,2,3</sup>, Min Liu <sup>1,2,3</sup>, Peng Zhou,<sup>4</sup> and Huigang Xiao<sup>1,2,3</sup>

<sup>1</sup>Key Lab of Intelligent Disaster Mitigation and Control for Civil Infrastructure, Harbin Institute of Technology, Harbin 150090, China

<sup>2</sup>Key Lab of Structures Dynamic Behavior and Control of the Ministry of Education, Harbin Institute of Technology, Harbin 150090, China

<sup>3</sup>School of Civil Engineering, Harbin Institute of Technology, Harbin 150090, China

<sup>4</sup>State Key Laboratory for Geomechanics & Deep Underground Engineering, School of Mechanics and Civil Engineering, China University of Mining and Technology, Xuzhou 221116, China

Correspondence should be addressed to Min Liu; liumin@hit.edu.cn

Received 6 October 2023; Revised 28 November 2023; Accepted 13 January 2024; Published 6 February 2024

Academic Editor: Łukasz Jankowski

Copyright © 2024 Junping Du et al. This is an open access article distributed under the Creative Commons Attribution License, which permits unrestricted use, distribution, and reproduction in any medium, provided the original work is properly cited.

As the stay cables of cable-stayed bridges become longer, parametric resonance with a large amplitude is more easily triggered, which becomes a vibration hazard of super-long stay cables. An increasing number of practical applications of vibration mitigation on stay cables demonstrate that vibration control strategies can effectively facilitate hazard mitigation and improve cable-stayed bridge reliability and service life. This study proposes a semiactive control approach to reduce the parametric vibration of super-long stay cables in cable-stayed bridges installed with magnetorheological fluid damper (MRFD). First, using the cable's gravity sag curve equation, an equation governing the combined stay cable-bridge deck-damper control system was established to consider the effect of the chordwise force of cable gravity. Subsequently, a targeted LQR-based optimal active control law is proposed to provide the target control force in the semiactive control. The parametric influences on the performance of the LQR-based optimal active control were analysed to provide insight into the proposed control strategy. Since the semiactive control could achieve almost the same control efficacy of the targeted optimal active control, a semiactive control strategy employing MRFD is proposed to mitigate the parametric vibration of a super-long stay cable. Based on the proposed semiactive control strategy, the system was attached with the MRFD of the longest cable, S36, in the designed prototype long cable-stayed bridge. The efficacy of the established semiactive control system was also analysed. The analysis results confirm that the proposed semiactive control strategy and designed semiactive control system can perform similar to the LQR-based optimal active control. The semiactive control system attached to the MRFD can mitigate the parametric vibration of super-long stay cables in cable-stayed bridge engineering practice.

## 1. Introduction

Cable-stayed bridges are prominent in modern long-span bridge structures because of their great spanning ability, graceful appearance, and wind-resistant stability. As essential structural bearing component in cable-stayed bridges, stay cables play an important role. The dynamic performance of stay cables affects the service status of cable-

stayed bridges. One of the major ways stay cables affect cable-stayed bridges is the large-amplitude parametric vibration of the stay cables. In contrast to forced vibration, the parametric vibration of stay cables is support-induced motion due to a bridge deck or tower vibration when cable-stayed bridges are under external excitations, such as wind, traffic load, and earthquakes. Frequent vibrations can lead to the fatigue fracture of the anchor ends of stay cables

and may cause the failure of stay cables in severe cases, which seriously impacts the safety and durability of cable-stayed bridges [1–4].

Several scholars have studied the parametric vibrations of cables. The excitation triggered by the parametric vibration of the stay cables can be divided into two cases according to the excitation. One is ideal excitation, in which the quality of the bridge deck or tower is much greater than that of the cable; consequently, the coupling interaction between the cable and bridge deck/tower can be neglected. The second is the nonideal excitation case. For this case, cable-bridge deck/tower coupling effects are considered, and the amplitude and frequency of the excitation vary with time. For ideal excitation, Tagata [5] and Lilien and Dacosta [6] ignored the effect of the gravity sag of the cable and derived the parametric vibration equations of cables under an axial ideal cosine excitation. Perkins [7] and Warnitchai et al. [8] used a quadratic parabola as the cable gravity sag curve when the parametric vibration equations of the cables were established under the end ideal displacement excitation. For nonideal excitation, the parametric vibration system varies with time and is nonautonomous [9, 10]. Xia and Fujino [11], Kang et al. [12], Yu et al. [13], and Wei et al. [14] established a coupled cable-bridge deck/tower parametric vibration system under nonideal excitation. They demonstrated that the cable-bridge coupling effects could enhance the nonlinear behavior of the parametric vibration.

The length and flexibility of stay cables increase continuously with the span of cable-stayed bridges, and with that comes the risk of large-amplitude parametric vibration [15]. It was found that if the inherent frequencies of the stay cable and bridge deck are close to a certain range, the large-amplitude parametric resonance of the cable would occur easily [16]. Through field measurements, it was observed that when the cable's local vibration frequency and the bridge's overall vibration frequency were close to 1 : 1, clear coupling stay cable-bridge deck parametric vibrations and corresponding strong interactions were observed and measured on International Guadiana Bridge [17] and Fred Hartman Bridge [18], respectively. Numerical analysis on the super-span cable-stayed bridge Sutong Bridge with a main span of 1088 m showed that it was easy for the cable to generate large-amplitude parametric vibrations [19]. With the span of the bridge deck and the length of the stay cable increasing, the stiffness and natural frequency of the stay cable decrease, and vibration inherent frequencies of both the bridge deck and stay cable are low and close-spaced, leading the range of modal frequency corresponding to the parametric vibration to widen, which makes it easy for the large-amplitude parametric resonance to arise under external excitation. Consequently, in terms of super-span cable-stayed bridges, inducing the large-amplitude parametric resonance of the cables becomes easier, thus reducing the durability of cable-stayed bridges. Currently, controlling the vibration of stay cables has become increasingly important to ensure the safety and durability of cable-stayed bridges. An appropriate control strategy can effectively mitigate the large-amplitude vibration of stay cables and improve the safety and long-term service life of cable-stayed

bridges. Therefore, studying and designing an effective control strategy to avoid large-amplitude parametric resonances are important.

Recently, novel control approaches are proposed during the rapid research development on vibration control of stay cables [20–24]. In terms of control devices, Gao et al. [21] proposed a novel design approach, in which the viscous inerter damper (VID) is regarded as a special output feedback control system, giving a high efficacy on mitigating multimode vibration mitigation of stay cables. Then, Gao and coauthors [22] further proposed a novel negative stiffness inerter damper (NSID), in which the damper can utilize simultaneously the damping enhancement of the negative stiffness and inerter for cable vibration control, thereby improving the control performance of stay cables. In terms of vibration control strategies, semiactive control is gaining popularity because it provides better control performance than passive control, which requires less external power than active control [25–36]. Ou and Li [37] proposed two principles for optimising the parameters of semiactive control devices and passive dampers; they used numerical simulations to determine the capacity of semiactive control required to achieve a performance similar to that of active control. With an intelligent control algorithm, a semiactive control device can consume a small amount of external energy to actively adjust its parameters according to the structural response while retaining outstanding control performance [38–42]. Shook et al. [39] proposed a superelastic, semiactive base isolation system that provides variable viscous damping that can be altered in real-time for the intelligent amelioration of the superstructure response. As a typical semiactive control device, the magnetorheological (MR) damper can easily achieve the targeted active control force amplitude [40, 43–47]. Recently, there have been new developments in the technique of MR damper [48, 49]. Jiang et al. [48] proposed a phenomenological model, which is more accurate in reflecting the dynamic characteristics of fluid-deficient MR dampers. Wang et al. [49] proposed a modified mechanical model, thereby improving the accuracy in describing the mechanical behavior of used MR dampers.

Up to now, as the world's first magnetorheological (MR) smart damping system in bridge structures has been installed for rain-wind-induced cable vibration control on the cable-stayed Dongting Lake Bridge, China [46], intelligent semiactive control adopting MR dampers, including magnetorheological fluid dampers (MRFDs), has been widely used to suppress large-amplitude vibrations of stay cables in cable-stayed bridges [46, 50–55]. Li et al. [50] used MRFD to control the stay cable vibration of the Yellow River Highway Bridge in Binzhou, Shandong Province, and proposed an innovative control algorithm based on a measurable acceleration response at limited locations along a stay cable. By employing a semiactive control algorithm, Wu and Cai [51] experimentally demonstrated that a semiactive MR damper achieves better control than a passive damper to mitigate cable vibration. Zhou et al. [53] proposed a semiactive control strategy based on the modulated homogeneous friction algorithm and verified its vibration reduction ability with optimally controlled MR dampers using a typical short cable as an example. Huang et al. [55] derived an efficient

semiactive control strategy in which the damping of the MR damper was tuned according to the dynamic characteristics of the stay cable to achieve the optimal damping of the cable damper system.

However, since the semiactive control is mainly used to suppress the wind/rain-induced vibration of stay cables in the previous research studies, there are hardly any studies on the semiactive control of parametric vibration of stay cables. Besides, the influence of the chordwise force of gravity of stay cables is usually ignored when establishing the parametric vibration model of stay cables [5–8, 11–14]. As the length of stay cables increases, the influence of the chordwise force of gravity increases. Through static analysis, it has been demonstrated that the physical quantities obtained by using the sag curve equation considering the chordwise force of gravity are the closest to the elastic catenary solutions, and the accuracy of the physical quantities is higher than that obtained by using parabola as the gravity sag curve equation [56]. Numerical results also showed that the influence of the chordwise force of gravity on the displacement response of parametric resonance gradually increases with the increase of the initial disturbance, and the chordwise force of gravity would amplify the displacement response of the main parametric resonance of stay cable [57]. Therefore, it is necessary to consider the effect of the chordwise force of gravity when establishing the parametric vibration model of the stay cable.

To this end, this study improves the design accuracy and control efficacy of the control system. Considering the influence of the chordwise force of gravity, a more accurate stay-cable parametric vibration model is established; the model provides an intelligent semiactive control strategy that effectively mitigates the large-amplitude parametric vibration of the coupled stay cable-bridge deck system. First, based on the gravity sag curve equation of the stay cable, including the chordwise force of gravity proposed by Liu et al. [58], the equation governing the parametric vibration of the coupled stay cable-bridge deck system is shown to have a sinusoidal excitation that directly acts on the bridge deck. Subsequently, a targeted LQR-based optimal active control law is proposed, which provides an optimal active control force. Subsequently, to optimise the active control force based on the branch-and-bound Hrovat optimal control algorithm [59], the study provides an intelligent semiactive control strategy for MRFD. Using the longest cable S36 in the prototype super-span cable-stayed bridge as an example, numerical simulations are used to compare

semiactive control with active control. The numerical results demonstrated that the semiactive control attached to the MRFD could provide control performance similar to that of the optimal active control and could effectively mitigate the parametric vibration of the super-long-stay cables in super-span cable-stayed bridges.

## 2. Theoretical Model of the Combined Stay Cable-Bridge Deck-Damper System

**2.1. Differential Equation Governing the Parametric Vibration.** As the span of the cable-stayed bridge increases, the coupling interaction between the stay cable and bridge deck becomes increasingly highlighted and cannot be neglected when the vibration of stay cables is studied. In the present study, considering the coupling interaction between the stay cable and the bridge deck, the differential equation of the stay-cable parametric vibration, including the chordwise force of gravity, was established with the following assumptions: (1) only considering the tensile stiffness of the stay cable, the cable's bending stiffness is neglected, (2) the bridge deck was simplified as a concentrated mass block, including stiffness and damping, and (3) the stay cable and bridge deck vibrate only in the gravity plane.

The combined stay cable-bridge deck-damper vibration control system is shown in Figure 1, where the  $x$  and  $y$  axes are the axial and lateral coordinates, respectively. A damper was installed close to the stay cable end, as shown in Figure 1, where  $x_d$  is the distance between the damper position and the end of the stay cable. The chord length of the stay cable was  $L$ , the mass per unit length of the stay cable was  $m$ , and the inclined angle of the chord from the horizontal was  $a$ . The mass, damping, stiffness, and natural frequency of the bridge deck block are denoted by  $M_b$ ,  $C_b$ ,  $K_b$ , and  $\omega_b$ , respectively. The external vertical excitation  $P(t)$  acts directly on the bridge deck, where  $P(t) = P_0 \cos(\theta t)$ .  $P_0$  and  $\theta$  are the amplitude and frequency of excitation, respectively. The vertical displacement of the bridge deck is  $d(t)$ . When the stay cable vibrates, the displacement from the axial and transverse equilibrium positions is  $u(x, t)$  and  $v(x, t)$ , respectively. The microsegment initial chord length and dynamic arc length of the cable are assumed as  $ds$  and  $dp$ , respectively, as shown in Figure 2.

According to Newton's second law, the nonlinear equation governing the in-plane transverse equilibrium of the combined stay cable-bridge deck-damper system is

$$\frac{\partial}{\partial p} \left[ (T_0 + T_d) \frac{\partial(f + v)}{\partial p} \right] dp = m \frac{\partial^2 v}{\partial t^2} dx + c \frac{\partial v}{\partial t} dx - mg \cos a dx + F_d(t) \frac{d\delta(x - L + x_d)}{dx}, \quad (1)$$

where  $T_0$  and  $T_d$  are the initial static tangential tension and additional tangential dynamic tension of the stay cable, respectively,  $f(x)$  is the gravity sag of the stay cable,  $\delta(\cdot)$  is the unit pulse function, and  $F_d(t)$  is the damping force from the damper. The gravity sag curve equation of the stay cable, including the chordwise force of gravity, is [58]

$$f(x) = \frac{mg \cos a}{2T_0} x(L - x) \left[ 1 - \frac{\lambda}{3} \left( 1 - 2 \frac{x}{L} \right) \right], \quad (2)$$

where  $\lambda = mgL \sin a / T_0$ , representing the proportion of the gravitational chord component to the initial tension of the cable. The initial chordal tension and additional chordal dynamic tension of the stay cable are  $H_0$  and  $H_d$ ,

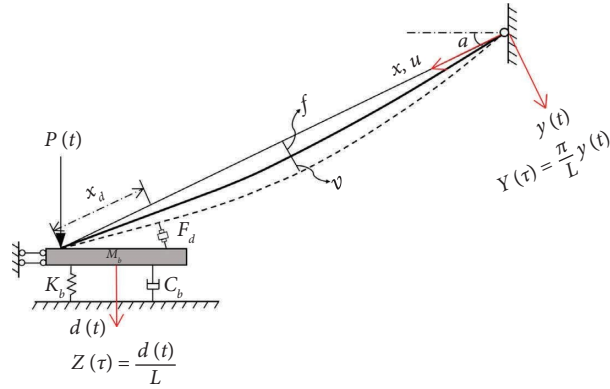


FIGURE 1: Modelling of the combined stay cable-bridge deck-damper system.

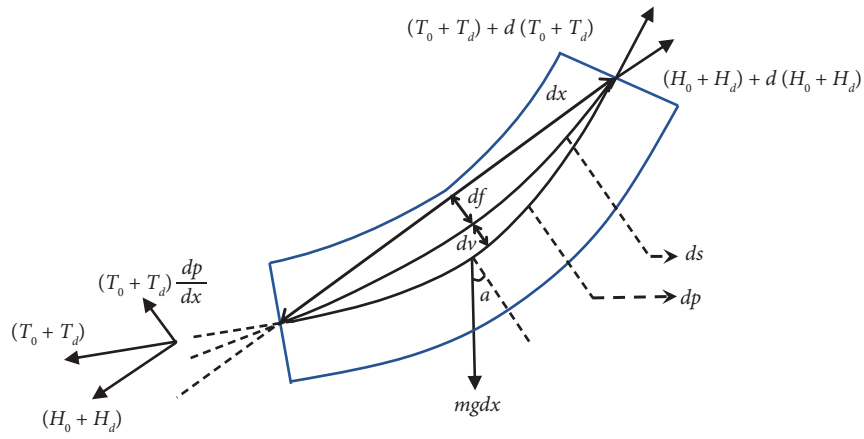


FIGURE 2: Schematic diagram of the microsegment of the stay cable.

respectively. According to the triangle similarity principle and the stay cable's static equilibrium [9], the in-plane vibration differential equation of the stay cable can be written as

$$(H_0 + H_d) \frac{\partial^2 v}{\partial x^2} + H_d \frac{d^2 f}{dx^2} = m \frac{\partial^2 v}{\partial t^2} + c \frac{\partial v}{\partial t} + F_d(t) \delta(x - L + x_d). \quad (3)$$

The additional chordal dynamic tension  $H_d$  can be obtained by taking the integral along the  $x$ -axis of  $dx$  over the chord length of the cable [9] as

$$H_d = \frac{EA}{L_e} \int_0^L \epsilon dx = \frac{EA}{L_e} \left[ D \cos(\theta t) + \int_0^L \frac{df}{dx} \frac{\partial v}{\partial x} dx + \frac{1}{2} \int_0^L \left( \frac{\partial v}{\partial s} \right)^2 dx \right], \quad (4)$$

$$L_e = \int_0^L \frac{dp}{dx} \left( \frac{ds}{dx} \right)^2 dx \approx \int_0^L \left( \frac{ds}{dx} \right)^3 dx \approx L \left[ 1 + 8 \left( \frac{R}{L} \right)^2 \right],$$

where  $L_e$  is the equivalent length, in which  $R = mgL \cos a / 8H_0$ , representing the ratio of the sag to span.

The vibration mode of the stay cable was approximated to be equal to that of a standard string. Considering sinusoidal excitation, the boundary conditions of the system were assumed as

$$\begin{aligned} u(0, t) &= v(0, t) = 0, \\ u(L, t) &= \sin a \cdot d(t), \\ v(L, t) &= \cos a \cdot d(t). \end{aligned} \quad (5)$$

The displacement of the stay cable from the transverse equilibrium position considering only the first vibration mode can be expressed as

$$\begin{aligned} v(x, t) &= v_1(x, t) + v_2(x, t) \\ &= \sin\left(\frac{\pi}{L}x\right)y(t) + \frac{x}{L}\cos a \cdot d(t), \end{aligned} \quad (6)$$

where  $y(t)$  is the generalised coordinate of the stay cable displacement from the transverse equilibrium position.

By substituting equations (2) and (6) into equation (4) and by integrating them,  $H_d$  becomes

$$H_d = \frac{EA}{L_e} \left( d(t) \sin a + \frac{16R}{\pi} y(t) + \frac{\pi^2}{4L} y(t)^2 + \cos^2 a \frac{d(t)^2}{2L^2} \right). \quad (7)$$

By substituting equations (2), (5), and (7) into equation (3) and processing the outcome with the Galerkin discretisation method, the differential equation governing the combined stay cable-bridge deck-damper system considering only the first mode is

$$\begin{aligned} \ddot{y}(t) + \frac{c}{m}\dot{y}(t) + \left( \frac{\pi^2 H_0}{mL^2} + \frac{512R^2 EA}{\pi^2 mL_e L^2} \right) y(t) + \frac{\pi^2 EA}{mL_e L^2} \left( \sin a d(t) + \frac{\cos^2 a}{2L^2} d(t)^2 \right) y(t) \\ + \frac{2 \cos a}{\pi} \dot{d}(t) + \frac{24\pi REA}{mL_e L^2} y(t)^2 + \frac{\pi^4 EA}{4mL_e L^3} y(t)^3 + \frac{32REA}{\pi mL_e L} \left( \sin a d(t) + \frac{\cos^2 a}{2L^2} d(t)^2 \right) \\ + \frac{2 \cos a}{\pi} \frac{c}{m} \dot{d}(t) + \frac{2F_d(t)}{mL} \sin(\pi(1 - \varepsilon_d)) = 0. \end{aligned} \quad (8)$$

The position of the exerted control force is defined as  $\varepsilon_d = x_d/L$ . The differential equilibrium equation of the bridge deck is written as follows:

$$M_b \ddot{d}(t) + C_b \dot{d}(t) + K_b d(t) + T_d \sin a = P(t). \quad (9)$$

Here,  $\dot{\bullet}$  and  $\ddot{\bullet}$  represent the first and second derivatives for actual time  $t$ , respectively.

For analysis, the following dimensionless parameters are introduced:

$\tau = \omega t$ ,  $Y(\tau) = \pi/L y(t)$ ,  $Z(\tau) = d(t)/L$ ,  $e = EA/H_0$ , and  $\iota = L/L_e$ .  $\bar{U}_{\varepsilon_d}(\tau)$  are the dimensionless generalised control force at the damper position, and  $\bar{U}_{\varepsilon_d}(\tau) = 2F_d(\varepsilon_d, \tau)/mL\omega$ ;

$\xi = c/2m\omega$  and  $\xi_b = C_b/2M_b\omega_b$  are the damping ratios of the stay cable and bridge deck, respectively.  $R_m = M_b/mL$  is the mass ratio of the bridge deck block to stay cable.  $\gamma_0 = \omega_0/\omega$ ,  $\gamma = \theta/\omega$ , and  $\gamma_b = \omega_b/\omega$  are the vibration frequency ratios of a standard string to the stay cable, excitation to the stay cable, and bridge deck to the stay cable, respectively, where  $\omega_0^2 = \pi^2 H_0/mL^2$ ,  $\omega^2 = \omega_0^2 (1 + (8\chi^2)/\pi^4 - (16e\iota R_s \sin 2a)/(\pi^4 R_m))$ , and  $\omega_b^2 = K_b/M_b + \iota EA \sin^2 a/M_b L$ , and  $\omega_0$ ,  $\omega$ , and  $\omega_b$  are the frequency of a standard string, stay cable, and bridge deck, respectively.

Equations (8) and (9) can be rewritten as

$$\begin{aligned} Y''(\tau) + 2\xi Y'(\tau) + Y(\tau) + (\alpha_1 Z(\tau) + \alpha_2 Z(\tau)^2) Y(\tau) + \alpha_3 Y(\tau)^2 + \alpha_4 Y(\tau)^3 \\ + \alpha_5 Z'(\tau) + \alpha_6 Z(\tau) + \alpha_7 Z(\tau)^2 + \bar{U}_{\varepsilon_d}(\tau) \sin(\pi(1 - \varepsilon_d)) + P_y \cos(\gamma\tau) = 0, \end{aligned} \quad (10a)$$

$$Z''(\tau) + 2\gamma_b \xi_b Z'(\tau) + \gamma_b^2 Z(\tau) + \alpha_8 Y(\tau) + \alpha_9 Y(\tau)^2 + \alpha_{10} Z(\tau)^2 = P_b \cos(\gamma\tau), \quad (10b)$$

where  $\bullet'$  and  $\bullet''$  represent the first and second derivative for the dimensionless time  $\tau$ ,  $\alpha_1 = \gamma_0^2 e \iota \sin a$ ,  $\alpha_2 = 1/2\gamma_0^2 e \iota \cos^2 a/L$ ,  $\alpha_3 = \gamma_0^2/\pi^2 (24e\iota R_s - e \iota \sin 2a/4R_m)$ ,  $\alpha_4 = 1/4e\iota \gamma_0^2$ ,  $\alpha_5 = 4 \cos a (\xi - \gamma_b \xi_b)$ ,  $\alpha_6 = 32e\iota R_s \sin a/\pi^2 \gamma_0^2 - 2\gamma_b^2 \cos a$ ,

$\alpha_7 = 3\gamma_0^2 e \iota \cos^2 a/\pi^2 (16R_s/L - \sin 2a/2R_m)$ ,  $\alpha_8 = 16e\iota R_s \gamma_0^2 \sin a/\pi^4 R_m$ ,  $\alpha_9 = e\iota \gamma_0^2 \sin a/4\pi^4 R_m$ ,  $\alpha_{10} = e\iota \gamma_0^2 \sin a \cdot \cos^2 a/2\pi^2 R_m L$ ,  $P_b = P_0 \gamma_0^2/\pi^2 R_m H_0$ , and  $P_y = 2P_0 \gamma_0^2 \cos a/\pi^2 R_m H_0$ .

Equations (10a) and (10b) are dimensionless differential equations that consider only the first vibration mode of the combined stay cable-bridge deck-damper active control system.

*2.2. LQR-Based Design Approach of the Active Control System.* In the state-space form, equations (10a) and (10b) can be rewritten as shown in equation (11) by neglecting nonlinear terms as follows:

$$\mathbf{z}'(\tau) = \mathbf{A}(\tau)\mathbf{z}(\tau) + \mathbf{D}F(\tau) + \mathbf{B}\bar{\mathbf{U}}_{\varepsilon_d}(\tau), \quad (11)$$

where

$$\mathbf{z}(\tau) = \begin{bmatrix} z_1(\tau) \\ z_2(\tau) \\ z_3(\tau) \\ z_4(\tau) \end{bmatrix} = \begin{bmatrix} Y(\tau) \\ Z(\tau) \\ Y'(\tau) \\ Z'(\tau) \end{bmatrix}, \quad (12a)$$

$$\mathbf{A} = \begin{bmatrix} 0 & 0 & 1 & 0 \\ 0 & 0 & 0 & 1 \\ -1 & -\alpha_6 & -2\xi & -\alpha_5 \\ -\alpha_8 & -\gamma_b^2 & 0 & -2\gamma_b\xi_b \end{bmatrix}, \quad (12b)$$

$$\mathbf{D} = \begin{bmatrix} 0 \\ 0 \\ -1 \\ \frac{P_b}{P_y} \end{bmatrix}, \quad (12c)$$

$$\mathbf{B} = \sin(\pi(1 - \varepsilon_d)) \cdot \begin{bmatrix} 0 \\ 0 \\ -1 \\ 0 \end{bmatrix}, \quad (12d)$$

$$F(\tau) = P_y \cos(\gamma\tau), \quad (12e)$$

$$\bar{\mathbf{U}}_{\varepsilon_d}(\tau) = \frac{2F_d(\varepsilon_d, \tau)}{mL\omega}, \quad (12f)$$

where  $\mathbf{z}(\tau)$  is the state vector of the system,  $\mathbf{A}$  is the state matrix of the system,  $\mathbf{D}$  is the position matrix of the external excitation,  $\mathbf{B}$  is the position matrix of the control force, and

$\bar{\mathbf{U}}_{\varepsilon_d}(\tau)$  is the dimensionless generalised control force at the damper position.

In this study, a linear quadratic regulator (LQR) controller was studied for a coupled stay cable-bridge deck active control system. The linear quadratic optimal regulator is an active control theory that can enable active control systems to achieve the expected structural response reduction. The quadratic function  $J$  of the active control system is defined as follows [60]:

$$J = \int_{\tau_0}^{\infty} \left[ \mathbf{z}^T(\tau)\mathbf{Q}\mathbf{z}(\tau) + \bar{\mathbf{U}}_{\varepsilon_d}^T(\tau)\mathbf{R}\mathbf{U}_{\varepsilon_d}(\tau) \right] d\tau, \quad (13)$$

where  $\bar{\mathbf{U}}_{\varepsilon_d}(\tau)$  is the dimensionless generalised optimal active control force of the active controller and is given by

$$\bar{\mathbf{U}}_{\varepsilon_d}(\tau) = -\mathbf{R}^{-1}\mathbf{B}^T\mathbf{P}\mathbf{z}(\tau), \quad (14)$$

where  $\mathbf{Q}$  and  $\mathbf{R}$  are the weight matrices expressed by diagonal matrices and  $\mathbf{P}$  is a symmetric positive definite matrix and the solution of the following algebraic Riccati equation:

$$-\mathbf{P}\mathbf{A} - \mathbf{A}^T\mathbf{P} + \mathbf{P}\mathbf{B}\mathbf{R}^{-1}\mathbf{B}^T\mathbf{P} - \mathbf{Q} = 0. \quad (15)$$

The generalised active control force  $\bar{\mathbf{U}}_{\varepsilon_d}(\tau)$  can be determined by minimising the performance index  $J$ . By combining the stay cable properties, the forms of  $\mathbf{Q}$  and  $\mathbf{R}$  are given by

$$\mathbf{Q} = \alpha \begin{bmatrix} 10 & 5(\alpha_6 + \alpha_8) & 0 & 0 \\ 5(\alpha_6 + \alpha_8) & 10\gamma_b^2 & 0 & 0 \\ 0 & 0 & 1 & 0 \\ 0 & 0 & 0 & 1 \end{bmatrix}, \quad (16a)$$

$$\mathbf{R} = \beta\mathbf{I}, \mathbf{I} = \text{identity matrix}, \quad (16b)$$

where  $\alpha$  and  $\beta$  are the weight matrix coefficients. We define  $\mathbf{P}$  as

$$\mathbf{P} = \begin{bmatrix} P_{11} & P_{21} & P_{31} & P_{41} \\ P_{21} & P_{22} & P_{32} & P_{42} \\ P_{31} & P_{32} & P_{33} & P_{34} \\ P_{41} & P_{42} & P_{34} & P_{44} \end{bmatrix}. \quad (17)$$

By substituting equations (12d), (16a), (16b), and (17) into equation (14) and considering only the first mode, the dimensionless generalised optimal active control force  $\bar{\mathbf{U}}_{\varepsilon_d}(\tau)$  of the active controller is calculated as

$$\bar{\mathbf{U}}_{\varepsilon_d}(\tau) = \beta^{-1} (P_{31}Y(\tau) + P_{32}Z(\tau) + P_{33}Y'(\tau) + P_{34}Z'(\tau))\sin(\pi(1 - \varepsilon_d)). \quad (18)$$

The dimensionless generalised control force  $\bar{U}_{\varepsilon_d}(\tau)$  is composed of elastic and damping forces. Thus,  $\bar{U}_{\varepsilon_d}(\tau)$  can be described by using the equivalent stiffness and damping coefficients as

$$\bar{U}_{\varepsilon_d}(\tau) = (k_{p1}V_{\varepsilon_d1}(\tau) + k_{p2}V_{\varepsilon_d2}(\tau) + c_{p1}V_{\varepsilon_d1}'(\tau) + c_{p2}V_{\varepsilon_d2}'(\tau)), \quad (19)$$

where  $V_{\varepsilon_d1}(\tau)$  and  $V_{\varepsilon_d2}(\tau)$  are the dimensionless transverse displacements of the stay cable and bridge deck at the damper installation location;  $k_{p1}$  and  $k_{p2}$  are the equivalent stiffness coefficients of the cable and bridge deck; and  $c_{p1}$  and

$c_{p2}$  are the equivalent damping coefficients of the cable and the bridge deck, respectively.

By using equation (6) and considering only the first mode, the dimensionless displacement and generalised control force of the installed damper can be expressed as

$$V_{\varepsilon_d}(\tau) = V_{\varepsilon_d1}(\tau) + V_{\varepsilon_d2}(\tau) = \sin(\pi(1 - \varepsilon_d))Y(\tau) + (1 - \varepsilon_d)\cos a \cdot Z(\tau), \quad (20)$$

$$\bar{U}_{\varepsilon_d}(\tau) = (K_{p1}Y(\tau) + K_{p2}Z(\tau) + C_{p1}Y'(\tau) + C_{p2}Z'(\tau)), \quad (21)$$

where

$$K_{p1} = k_{p1} \sin(\pi(1 - \varepsilon_d)), \quad (22a)$$

$$K_{p2} = k_{p2} (1 - \varepsilon_d) \cos a, \quad (22b)$$

$$C_{p1} = c_{p1} \sin(\pi(1 - \varepsilon_d)), \quad (22c)$$

$$C_{p2} = c_{p2} (1 - \varepsilon_d) \cos a. \quad (22d)$$

Suppose  $\bar{U}_{\varepsilon_d}(\tau)$  equals the dimensionless generalised optimal active control force  $\bar{U}_{\varepsilon_d|a}(\tau)$ , that is,  $\bar{U}_{\varepsilon_d}(\tau) = \bar{U}_{\varepsilon_d|a}(\tau)$ , then by considering equations (18), (20), (22a)–(22d), the expressions of  $K_{p1}$ ,  $K_{p2}$ ,  $C_{p1}$ ,  $C_{p2}$ ,  $k_{p1}$ ,  $k_{p2}$ ,  $c_{p1}$ , and  $c_{p2}$  are given as

$$K_{p1} = \beta^{-1}P_{31} \sin(\pi(1 - \varepsilon_d)), \quad (23a)$$

$$K_{p2} = \beta^{-1}P_{32} \sin(\pi(1 - \varepsilon_d)),$$

$$C_{p1} = \beta^{-1}P_{33} \sin(\pi(1 - \varepsilon_d)), \quad (23b)$$

$$C_{p2} = \beta^{-1}P_{34} \sin(\pi(1 - \varepsilon_d)),$$

$$k_{p1} = \beta^{-1}P_{31}, \quad (24a)$$

$$k_{p2} = \frac{\beta^{-1}P_{32} \sin(\pi(1 - \varepsilon_d))}{(1 - \varepsilon_d)\cos a},$$

$$c_{p1} = \beta^{-1}P_{33}, \quad (24b)$$

$$c_{p2} = \frac{\beta^{-1}P_{34} \sin(\pi(1 - \varepsilon_d))}{(1 - \varepsilon_d)\cos a}.$$

According to equations (24a), (24b), and (19), the values of  $P_{31}$ ,  $P_{32}$ ,  $P_{33}$ , and  $P_{34}$  can directly determine the equivalent stiffness and damping coefficients, thereby influencing the active control force. In addition, equation (15) shows that  $P_{31}$ ,  $P_{32}$ ,  $P_{33}$ , and  $P_{34}$  can be determined from the ratio of  $\beta$  to  $\alpha$ . Thus, the ratio of  $\beta$  to  $\alpha$  plays an essential role in the active control force. Obtaining an appropriate value of  $\beta/\alpha$  is critical for achieving the expected control performance.

If equation (21) is substituted into equations (10a) and (10b), then equations (10a) and (10b) are represented as

$$\begin{aligned} Y''(\tau) + 2\xi Y'(\tau) + Y(\tau) + (\alpha_1 Z(\tau) + \alpha_2 Z(\tau)^2)Y(\tau) \\ + \alpha_3 Y(\tau)^2 + \alpha_4 Y(\tau)^3 + \alpha_5 Z'(\tau) + \alpha_6 Z(\tau) \\ + \alpha_7 Z(\tau)^2 + \sin(\pi(1 - \varepsilon_d)) \cdot (K_{p1}Y(\tau) + K_{p2}Z(\tau) \\ + C_{p1}Y'(\tau) + C_{p2}Z'(\tau)) + P_y \cos(\gamma\tau) = 0, \end{aligned} \quad (25a)$$

$$\begin{aligned} Z''(\tau) + 2\gamma_b \xi_b Z'(\tau) + \gamma_b^2 Z(\tau) + \alpha_8 Y(\tau) \\ + \alpha_9 Y(\tau)^2 + \alpha_{10} Z(\tau)^2 = P_b \cos(\gamma\tau). \end{aligned} \quad (25b)$$

The expressions for the parameters in equations (25a) and (25b) are the same as those listed in Section 2.1.

**2.3. Bingham Model of the MRFD and the Optimal Semiactive Control Algorithm.** In this study, the Bingham model proposed by Stanway et al. was adopted to describe the damping force of the MRFD, as shown in the following equation:

$$F(t) = f_d(t) \operatorname{sgn}(\dot{x}_d) + c_d \dot{x}_d, \quad (26)$$

where  $f_d(t)$  is the adjustable Coulomb damping force of the MRFD,  $\operatorname{sgn}(\cdot)$  is the sign function,  $\dot{x}_d$  is the velocity of the MRFD location, and  $c_d$  is the viscous damping coefficient of the MRFD.

Utilising the branch-and-bound Hrovat optimal semi-active control algorithm on the Bingham dynamic model, the dimensionless generalised semiactive control force  $\bar{U}_{\varepsilon_d|s}(\tau)$  of the MRFD can be expressed as

$$\bar{U}_{\varepsilon_d|s}(\tau) = \begin{cases} -\bar{c}_d V'_{\varepsilon_d}(\tau) - \bar{f}_{d\max} \text{sgn}[V'_{\varepsilon_d}(\tau)], & \bar{U}_{\varepsilon_d|s}(\tau) \cdot V'_{\varepsilon_d}(\tau) < 0 \text{ and } |\bar{U}_{\varepsilon_d|a}(\tau)| > \bar{U}_{\varepsilon_d|s}(\tau)_{\max}, \\ -|\bar{U}_{\varepsilon_d|a}(\tau)|, & \bar{U}_{\varepsilon_d|s}(\tau) \cdot V'_{\varepsilon_d}(\tau) < 0 \text{ or } |\bar{U}_{\varepsilon_d|a}(\tau)| < \bar{U}_{\varepsilon_d|s}(\tau)_{\max}, \\ -\bar{c}_d V'_{\varepsilon_d}(\tau) - \bar{f}_{d\min} \text{sgn}[V'_{\varepsilon_d}(\tau)], & \bar{U}_{\varepsilon_d|a}(\tau) \cdot V'_{\varepsilon_d}(\tau) \geq 0, \end{cases} \quad (27)$$

where  $V'_{\varepsilon_d}(\tau)$  is the dimensionless relative velocity when  $x = x_d$ , that is, the velocity at the MRFD location, where  $V'_{\varepsilon_d}(\tau) = \sin(\pi(1 - \varepsilon_d))Y'(\tau) + \varepsilon_d \cdot \cos a \cdot Z'(\tau)$  according to equation (6);  $\bar{c}_d$  is the dimensionless viscous damping coefficient of MRFD;  $\bar{f}_{d\max}$  and  $\bar{f}_{d\min}$  are the dimensionless maximum and minimum Coulomb damping forces of MRFD; and  $\bar{U}_{\varepsilon_d|a}(\tau)$  expressed in equation (18) is the dimensionless generalised active optimal control force.

In addition, the bang-bang control algorithm is also utilized to give a comparison analysis with the branch-and-bound Hrovat optimal semiactive control algorithm. Based on the bang-bang control algorithm, the dimensionless generalised semiactive control force  $\bar{U}_{\varepsilon_d|B}(\tau)$  can be expressed as

$$\bar{U}_{\varepsilon_d|B}(\tau) = \begin{cases} -\bar{c}_d V'_{\varepsilon_d}(\tau) - \bar{f}_{d\max} \text{sgn}[V'_{\varepsilon_d}(\tau)], & \bar{U}_{\varepsilon_d|B}(\tau) \cdot V'_{\varepsilon_d}(\tau) < 0, \\ -\bar{c}_d V'_{\varepsilon_d}(\tau) - \bar{f}_{d\min} \text{sgn}[V'_{\varepsilon_d}(\tau)], & \bar{U}_{\varepsilon_d|B}(\tau) \cdot V'_{\varepsilon_d}(\tau) \geq 0. \end{cases} \quad (28)$$

Suppose that the generalised control force  $\bar{U}_{\varepsilon_d}(\tau)$  in equations (10a) and (10b) is equal to the dimensionless generalised semiactive control force  $\bar{U}_{\varepsilon_d|s}(\tau)$ , that is

$\bar{U}_{\varepsilon_d}(\tau) = \bar{U}_{\varepsilon_d|s}(\tau)$ , then by substituting  $\bar{U}_{\varepsilon_d|s}(\tau)$  in equations (10a) and (10b), equations (10a) and (10b) can be rewritten as

$$Y''(\tau) + 2\xi Y'(\tau) + Y(\tau) + (\alpha_1 Z(\tau) + \alpha_2 Z(\tau)^2)Y(\tau) + \alpha_3 Y(\tau)^2 + \alpha_4 Y(\tau)^3 + \alpha_5 Z'(\tau) + \alpha_6 Z(\tau) + \alpha_7 Z(\tau)^2 - \sin(\pi(1 - \varepsilon_d)) \cdot \bar{U}_{\varepsilon_d|s}(\tau) + P_y \cos(\gamma\tau) = 0, \quad (29a)$$

$$Z''(\tau) + 2\gamma_b \xi_b Z'(\tau) + \gamma_b^2 Z(\tau) + \alpha_8 Y(\tau) + \alpha_9 Y(\tau)^2 + \alpha_{10} Z(\tau)^2 = P_b \cos(\gamma\tau). \quad (29b)$$

**2.4. Parameter Design of MRFD.** As stated above, a targeted optimal active control law was first designed for the coupled stay cable-bridge deck system. If the semiactive control strategy can emulate the targeted optimal active control efficacy, then the semiactive control can achieve the maximum optimal control force. Hence, the maximum damping force of the MRFD (including the passive viscous and Coulomb damping forces) should be designed according to the targeted maximum optimal active control force. To

compare semiactive control with optimal active control, we let the maximum semiactive control force of the MRFD to be equal to the corresponding maximum active control force. The semiactive control attached to the MRFD of the coupled stay cable-bridge deck system is assumed to achieve the same control efficacy as the optimal active control system. Thus, the maximum dimensionless generalised control force can be expressed as

$$\bar{U}_{\varepsilon_d|s\max}(\tau) = -\bar{c}_d \left| V'_{s|\bar{U}_{\varepsilon_d|s\max}}(\tau) \right| - \bar{f}_{d\max} = -\bar{c}_d \left| V'_{a|\bar{U}_{\varepsilon_d|a\max}}(\tau) \right| - \bar{f}_{d\max} = \bar{U}_{\varepsilon_d|a\max}(\tau), \quad (30)$$



where  $\bar{U}_{\varepsilon_d|s\max}(\tau)$  and  $\bar{U}_{\varepsilon_d|a\max}(\tau)$  are the maximum dimensionless generalised semiactive control force and optimal active control force and  $|V'_{s|\bar{U}_{\varepsilon_d|s\max}}(\tau)|$  and  $|V'_{a|\bar{U}_{\varepsilon_d|a\max}}(\tau)|$  are the dimensionless relative in-plane transverse velocity at the damper location corresponding to the maximum

$$\bar{U}_{\varepsilon_d|s\max}(\tau) = -s\bar{c}_d \left| V'_{s|\bar{U}_{\varepsilon_d|s\max}}(\tau) \right| = -s\bar{c}_d \left| V'_{a|\bar{U}_{\varepsilon_d|a\max}}(\tau) \right| = \bar{U}_{\varepsilon_d|a\max}(\tau). \quad (31)$$

Then, the dimensionless passive viscous damping coefficient of the MRFD is

$$\bar{c}_d = \left| \frac{\bar{U}_{\varepsilon_d|a\max}(\tau)}{\left( s \cdot V'_{a|\bar{U}_{\varepsilon_d|a\max}}(\tau) \right)} \right|. \quad (32)$$

Using equations (30) and (31), the dimensionless maximum Coulomb damping force of the MRFD is

$$\bar{f}_{d\max}(s-1)\bar{c}_d \left| V'_{s|\bar{U}_{\varepsilon_d|s\max}}(\tau) \right| = (s-1)\bar{c}_d \left| V'_{a|\bar{U}_{\varepsilon_d|a\max}}(\tau) \right|. \quad (33)$$

To provide insight into the physical parameters of the designed MRFD, the physical passive viscous damping coefficient  $c_d$  and the maximum Coulomb damping force  $f_{d\max}$  of the MRFD can be obtained as follows:

$$c_{d|e_d} = \frac{mL}{2} \cdot \bar{c}_d, \quad (34a)$$

$$f_{d\max} = \frac{mL}{2} \cdot \bar{f}_{d\max}. \quad (34b)$$

### 3. Numerical Analysis of the Coupled Stay Cable-Bridge Deck Active and Semiactive Control System

**3.1. Prototypical Stay Cable in Cable-Stayed Bridge.** For the analysis of the influence of parameters on the dynamic properties and control efficacy of the parametric vibration of the super-long stay cable, cable S36 in the Shanghai-Suzhou-Nantong Yangtze River Bridge was considered. The geometric parameters and material properties of stay cables are listed in Table 1. The classical fourth-order Runge–Kutta method is employed to solve the differential equations (25a), (25b), (29a), and (29b).

**3.2. Relation between the Weight Matrix Coefficient Ratio and Equivalent Stiffness/Damping Coefficients.** In this study, because the weight matrices  $\mathbf{Q}$  and  $\mathbf{R}$  are determined by the weight matrix coefficients  $\alpha$  and  $\beta$ , respectively, the control efficacy of the LQR controller is determined by the ratio of  $\beta$  and  $\alpha$ , that is,  $\beta/\alpha$ . As mentioned above, the generalised active control force  $\bar{U}_{\varepsilon_d|a}(\tau)$  is expressed by the equivalent stiffness coefficient  $k_{p1}$  and equivalent damping coefficient  $c_{p1}$  of the

semiactive control force of MRFD and maximum active control force, respectively.

This study assumes that the dimensionless minimum Coulomb damping force of the MRFD is zero and the adjustable multiple is represented by  $s$ , according to the following equation:

stay cable and the equivalent stiffness coefficient  $k_{p2}$  and equivalent damping coefficient  $c_{p1}$  of the bridge deck, which are shown in equations (24a) and (24b). To numerically investigate the relationship between the ratio  $\beta/\alpha$  and four equivalent coefficients, cable S36 in the prototype super-span cable-stayed bridge is taken as an example. The relationships between the ratio  $\beta/\alpha$  and equivalent coefficients  $k_{p1}$ ,  $k_{p2}$ ,  $c_{p1}$ , and  $c_{p2}$  obtained using the fourth-order Runge–Kutta algorithm are shown in Figure 3.

Figure 3 shows that the ratio  $\beta/\alpha$  decreases nonlinearly with an increase in the four equivalent coefficients. In addition, for a certain value of  $\beta/\alpha$ , the equivalent damping coefficient  $c_{p1}$  of the cable is much larger than the equivalent damping coefficient  $c_{p2}$  of the bridge deck, whereas the equivalent stiffness coefficient  $k_{p1}$  of the cable is approximately ten times the equivalent stiffness coefficient  $k_{p2}$  of the bridge deck.

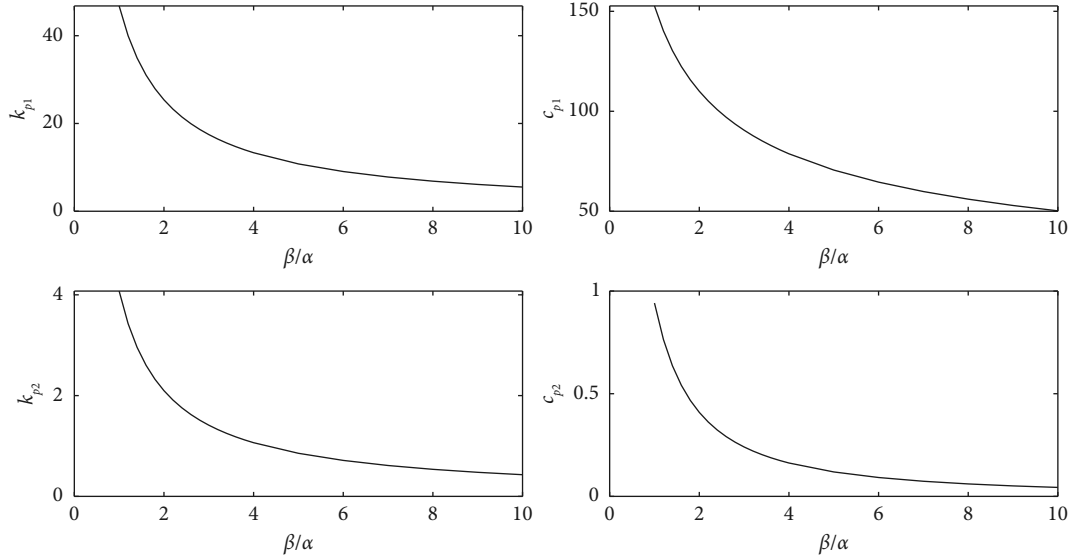
**3.3. Influence of Parameters on the Parametric Vibration of the Active Control System.** The influence of parameters on the parametric vibration of the coupled stay cable-bridge deck active control system, including the influence of parameters such as the frequency ratio of the bridge deck, stay cable, and external excitation  $\gamma_3 = \omega_b$ ;  $\omega$ :  $\theta$ , the optimal weight matrix coefficient ratio  $\beta/\alpha$ , and the characteristics of the active control force, was analysed with the coupled stay cable-bridge deck system and is operated under active control and sinusoidal excitation. To analyse the influence of the frequency ratio in more detail, the frequency ratios of the bridge deck to the stay cable  $\gamma_b = \omega_b/\omega$  and external excitation to the stay cable  $\gamma = \theta/\omega$  were established.

**3.3.1. Influence of the Frequency Ratios and Weight Matrix Coefficient Ratios.** For the super-long cable S36, the influence of the frequency ratio of the bridge deck to the stay cable  $\gamma_b = \omega_b/\omega$ , external excitation to the stay cable  $\gamma = \theta/\omega$ , and bridge deck-stay cable-excitation  $\gamma_3 = \omega_b$ ;  $\omega$ :  $\theta$  on the dynamic performance of the coupled stay cable-bridge deck is discussed first. For free vibration, that is, when  $P_0$  is zero, based on equations (25a) and (25b), the initial conditions are  $R_m = 100$ ,  $\xi = 0.002$ ,  $\xi_d = 0.01$ ,  $Z(\tau_0) = 0.05$ ,  $Z'(\tau_0) = 0$ ,  $Y(\tau_0) = 0.0001$ ,  $Y'(\tau_0) = 0$ , and  $P_0 = 0$ .

First, the frequency ratio of the bridge deck-stay cable  $\gamma_b$  is analysed. The relationship between the maximum displacement of the stay cable and frequency ratio of the bridge

TABLE 1: Parameters of a typical super-long stay cable.

Initial tension	Mass per unit length	Length	Inclination angle	Cross-sectional area	Young's modulus	Fundamental frequency
$H_0$	$m$	$L$	$\alpha$	$A$	$E$	$\omega/2\pi$
12183 kN	145.0 kg/m	594.35 m	26.48°	173.57 cm <sup>2</sup>	205 GPa	0.244 Hz

FIGURE 3: Relationships between the weight matrix coefficient ratio  $\beta/\alpha$  and equivalent coefficients  $k_{p1}$ ,  $k_{p2}$ ,  $c_{p1}$ , and  $c_{p2}$ .

deck-stay cable  $\gamma_b$  corresponding to the free vibration of the coupled stay cable-bridge deck system is shown in Figure 4. The figure shows three peaks corresponding to the frequency ratios  $\gamma_b$  of the bridge deck-stay cable of 0.504, 0.999, and 2.001, indicating that the stay cable exhibits 1:2 superharmonic resonance, 1:1 primary resonance, and 2:1 main parametric resonance when the frequency ratio of the bridge deck-stay cable is approximately 0.5, 1, and 2.

For the frequency ratios  $\gamma_b$  of the bridge deck-stay cable of 0.5, 1, and 2, the force amplitude of the forced vibration of the external excitation subjected to the bridge deck  $P_0$  is 80 kN. By some numerical trial calculations, it is found that the vibration response displacement of the stay cable would be too large when  $P_0 > 136$  kN, and too small when  $P_0 < 69.1$  kN. Since the paper focuses on the engineering practice, it is wanted that the value of the vibration response displacement of the cable is close to that in a real system of engineering analysis. Therefore, the representative 80 kN was chosen as the excitation amplitude  $P_0$ , which can arise a proper vibration response of cable, making it appropriate for engineering practice. The initial values of the parameters were identical to those of the free vibration. The frequency ratio  $\gamma$  of the external excitation-stay cable was then analysed. The relationship between the maximum displacement of the stay cable/bridge deck and frequency ratio  $\gamma$  of the external excitation-stay cable are shown in Figure 5.

As shown in Figure 5(a), when the frequency ratio  $\gamma_b$  of the bridge deck-stay cable is approximately 0.5, as marked with the red curve, there are peaks corresponding to the

frequency ratios  $\gamma$  approximately, indicating that there are large displacement amplitudes when the frequency ratio of the bridge deck, stay cable, and external excitation  $\gamma_3 = \omega_b: \omega: \theta$  is approximately 1:2:1 and 1:2:2, respectively. In other words, the external excitation resonates with the same and twice to that of the frequency of the bridge deck, and the stay cable exhibits a 1:2 superharmonic resonance. Similarly, the blue and yellow curves in Figure 5(a) show that the maximum displacement response amplitude at the midspan of the stay cable under the external sinusoidal excitation occurs when the frequency ratio of the bridge deck, stay cable, and external excitation  $\gamma_3 = \omega_b: \omega: \theta$  is approximately 1:2:1, 1:2:2, 1:1:1, 2:1:1, and 2:1:2. In other words, the external excitation resonates with half, same, and twice the frequency of the bridge deck, and simultaneously, the stay cable exhibits a 1:2 superharmonic resonance, 2:1 main parametric resonance, or 1:1 primary resonance.

For the vibration of the bridge deck, as shown in Figure 5(b), the peak displacement amplitude of the bridge deck for the frequency ratio of the bridge deck, stay cable, and external excitation  $\gamma_3 = \omega_b: \omega: \theta$  of approximately 1:2:1 is the maximum, followed by the displacement response for the frequency ratios  $\gamma_3 = \omega_b: \omega: \theta$  of approximately 1:1:1 and 2:1:2, respectively. Owing to the super-span cable-stay bridge with small stiffness and large flexibility, the natural frequency of the bridge deck is small, and consequently, the resonant response is significantly increased. Therefore, considering the bridge deck's vibration, mitigating the stay cable's large-amplitude vibration is crucial.

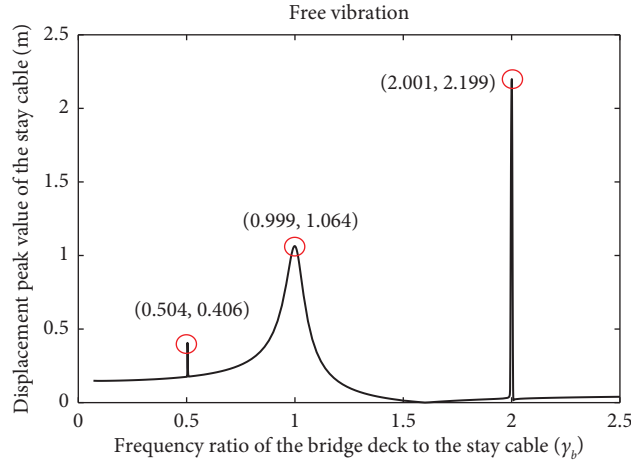


FIGURE 4: Relation of the maximum displacement of the stay cable and frequency ratio  $\gamma_b$  corresponding to the free vibration of the coupled stay cable-bridge deck system.

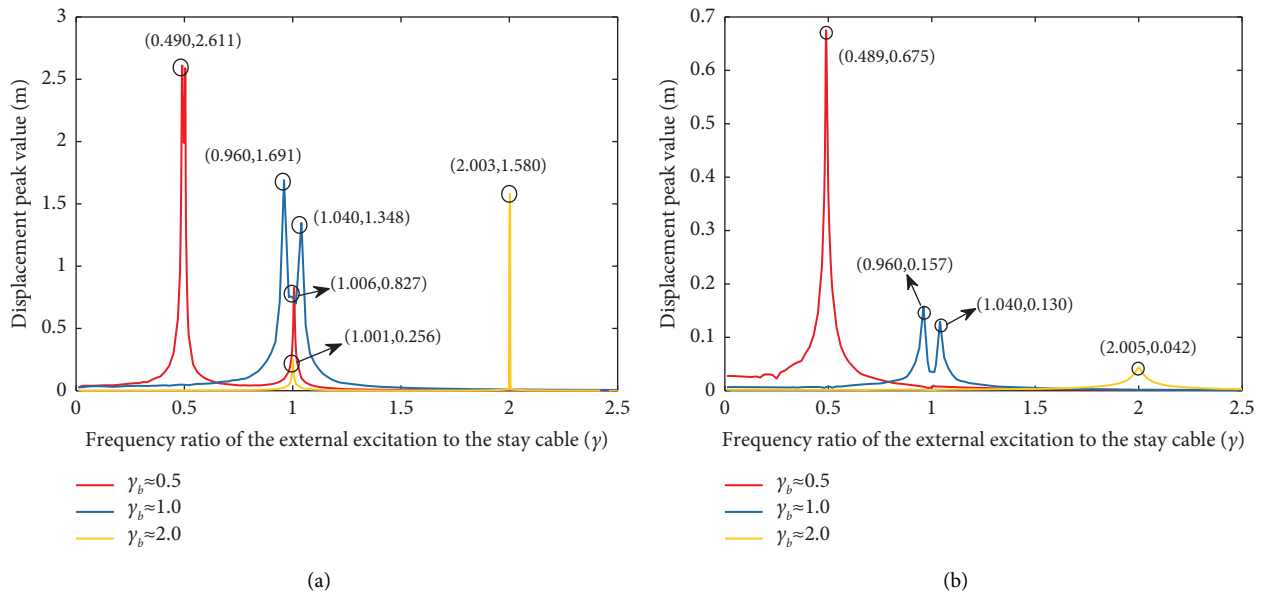


FIGURE 5: Relationship between the maximum displacement response of the stay cable/bridge deck and frequency ratio  $\gamma$  corresponding to the forced vibration without control: (a) at the midspan of the stay cable and (b) at the bridge deck.

Then, the frequency-amplitude characteristics of the coupled stay cable-bridge deck system operated with active control were analysed. Figure 6 shows the relationship between the maximum displacement of the stay cable/bridge deck and the frequency ratio  $\gamma$  of the external excitation to the stay cable when the coupled stay cable-bridge deck system has active control. Figure 6 shows that when the optimal active control force with different weight matrix coefficient ratios  $\beta/\alpha$  is exerted on the coupled stay cable-bridge deck system, the peak displacement responses at the midspan of the stay cable only exist with the frequency ratios of the bridge deck, stay cable, and external excitation  $\gamma_3 = \omega_b: \omega: \theta$  of approximately 1:2:1 and 1:1:1, and the peak values of the displacement are decreased significantly compared with those shown in Figure 5(a). For the bridge deck, the frequency ratios of the bridge deck, stay cable, and

external excitation  $\gamma_3 = \omega_b: \omega: \theta$  corresponding to the resonance are close to those without control, and the resonance displacement amplitudes decrease slightly compared to those without control, as shown in Figure 6(b). For the frequency ratios of the bridge deck, stay cable, and external excitation  $\gamma_3 = \omega_b: \omega: \theta$  of approximately 1:2:1 and 1:1:1, respectively, there is only one peak displacement response.

3.3.2. *Optimal Design Weight Matrix Coefficient Ratio and Characteristics of the Maximum Active Control Force.* For the different frequency ratios  $\gamma_3$  and to choose the optimal weight matrix coefficient ratio  $\beta/\alpha$ , the relationship between the active control efficacies on the midspan displacement of stay cable S36 and weight matrix coefficient ratios  $\beta/\alpha$  of the coupled stay cable-bridge deck active

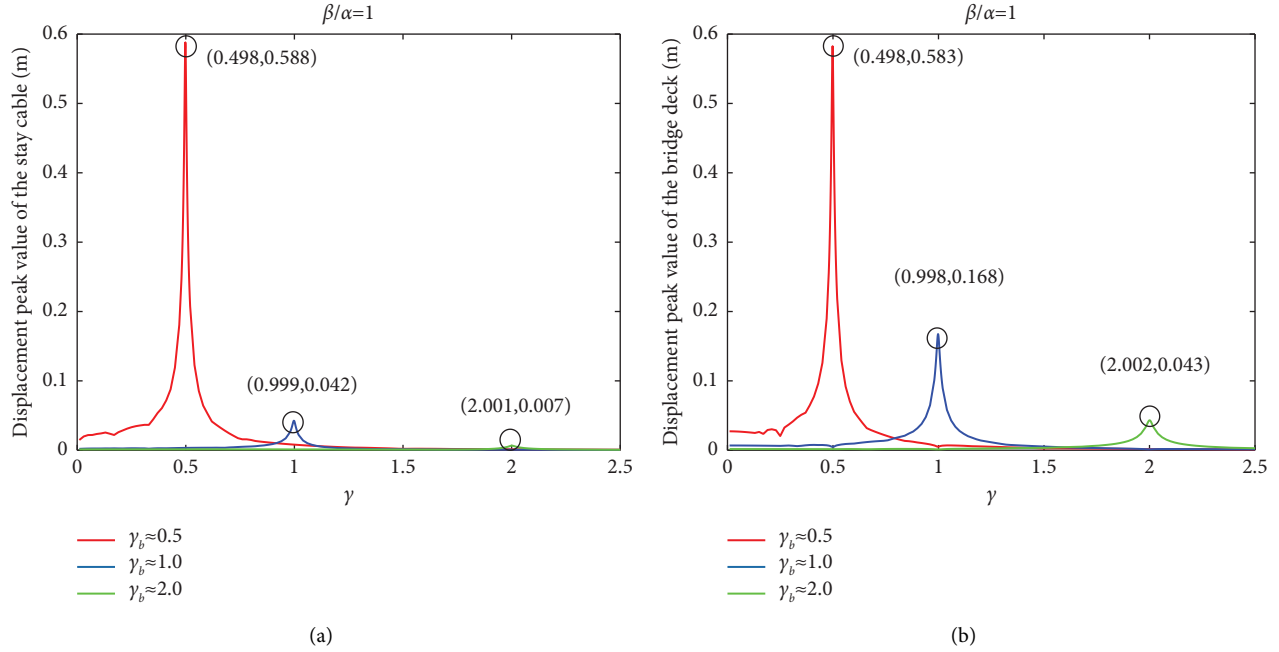


FIGURE 6: Relationship between the maximum displacement response of the stay cable/bridge deck and frequency ratio  $\gamma$  corresponding to the forced vibration under active control: (a) at the midspan of the stay cable and (b) at the bridge deck.

control system is analysed, as shown in Figure 7. The characteristics of the LQR-based active control force exerted on the coupled stay cable-bridge deck system were analysed, as shown in Figures 8 and 9.

Figure 7 shows that as the weight matrix coefficient ratio  $\beta/\alpha$  increases, the control efficacy decreases sharply and then decreases slowly. For  $\gamma_3 = \omega_b$ :  $\omega$ :  $\theta \approx 2:1:2$ , the active control efficacy is maximised, reaching 99%. In addition, the control efficacy decreases slightly as the weight matrix coefficient ratio  $\beta/\alpha$  decreases, indicating that the active control strategy is highly efficient and stable for the main parametric resonance. The same variation trend is observed for the curves of the maximum control force  $F_{d\max}$  of stay cable S36 and the weight matrix coefficient ratios  $\beta/\alpha$  of the coupled stay cable-bridge deck active control system are shown in Figure 8. In addition, when the weight matrix coefficient ratio  $\beta/\alpha$  decreased to a certain value, the maximum active control force  $F_{d\max}$  tended to be stable.

Figure 9 shows the relationship between the maximum control force  $F_{d\max}$  and control efficacies of the midspan displacement of the stay cable of the coupled stay cable-bridge deck active control system. The larger the maximum actual control force  $F_{d\max}$ , the larger the control efficacy, which is consistent with the relationship between the control force and efficacy of the active control system.

The analysis in Sections 3.3.1 clarifies that control efficacy and force should be considered when choosing the appropriate value of the optimal weight matrix coefficient ratio  $\beta/\alpha$ . After comprehensive considerations, the optimal weight matrix coefficient ratio  $\beta/\alpha$  was determined to be  $\beta/\alpha = 1$ .  $\beta/\alpha = 1$  indicates that the control efficacy and force of the coupled stay cable-bridge deck active control system are effective and moderate.

### 3.4. Discussions of Semiactive Control of the Coupled Stay Cable-Bridge Deck Attached with MRFD

3.4.1. Numerical Analysis on the Semiactive Control of the System Attached with MRFD. Based on the numerical analysis of the coupled stay cable-bridge deck active control system, utilising equations (31)–(34a) and (34b) and taking the super-long stay cable S36 as an example, the parameters of the MRFD installed at a 3% distance from the support were designed, and the semiactive control of the coupled stay cable-bridge deck system was numerically analysed.

According to Section 3.3.1, the optimal design weight matrix coefficient ratio  $\beta/\alpha$  of the optimal active control was determined as  $\beta/\alpha = 1$ . For the superharmonic resonance with  $\gamma_3 = \omega_b$ :  $\omega$ :  $\theta = 1:2:1$ , primary resonance with  $\gamma_3 = \omega_b$ :  $\omega$ :  $\theta = 2:1:2$ , and main parametric resonance with  $\gamma_3 = \omega_b$ :  $\omega$ :  $\theta = 1:1:1$ , the maximum dimensionless generalised active and physical control forces can be obtained, which are represented by  $\bar{U}_{\varepsilon_d|a\max}(\tau)$  and  $U_{d\max}$ , respectively. For the maximum dimensionless active control force  $\bar{U}_{\varepsilon_d|a\max}(\tau)$ , the in-plane transverse relative velocity  $|V'_{a|\bar{U}_{a\max}}(\varepsilon_d, \tau)|$  of the active control system at the damper installation location can be obtained. According to the frequency ratios of the stay cable-bridge deck-external excitation, that is,  $\gamma_3 = \omega_b$ :  $\omega$ :  $\theta$ , which are  $1:2:1$ ,  $1:1:1$ , and  $2:1:2$ , the three sets of parameters of the MRFD are designed based on the branch-and-bound Hrovat algorithm according to equations (32) and (33) and labelled as para 1, para 2, and para 3, respectively, as shown in Table 2. Para 1-B, para 2-B, and para 3-B mean that the designed case is based on the bang-bang control algorithm. It should be noted that para 1-B, para 2-B, and para 3-B share the same

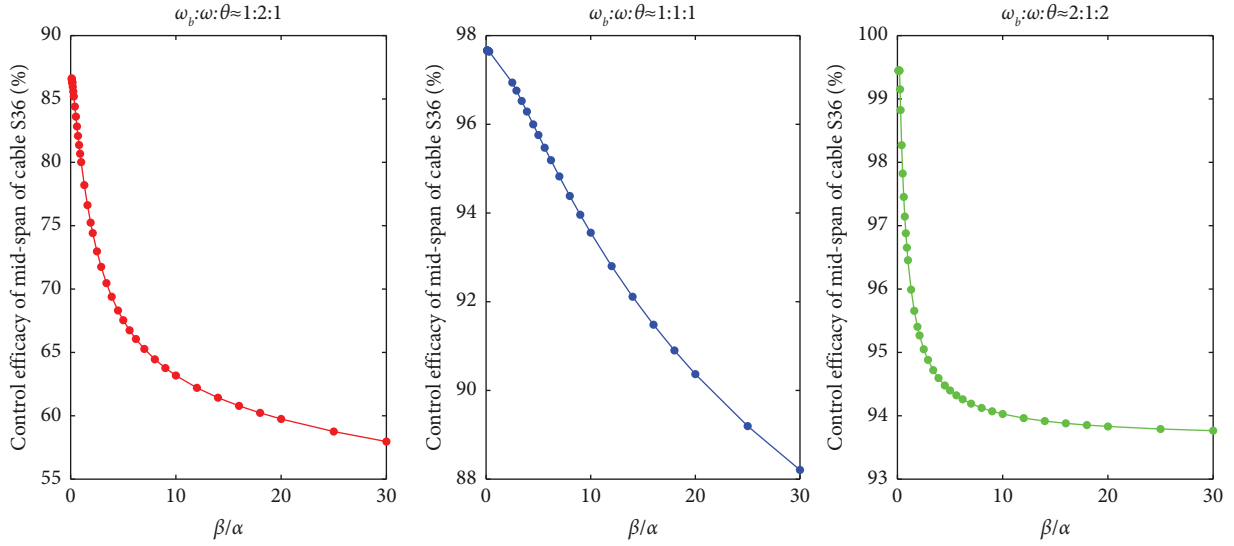


FIGURE 7: Relationship between the active control efficacies on the midspan displacement of the stay cable and the weight matrix coefficient ratios  $\beta/\alpha$  of the coupled stay cable-bridge deck active control system.

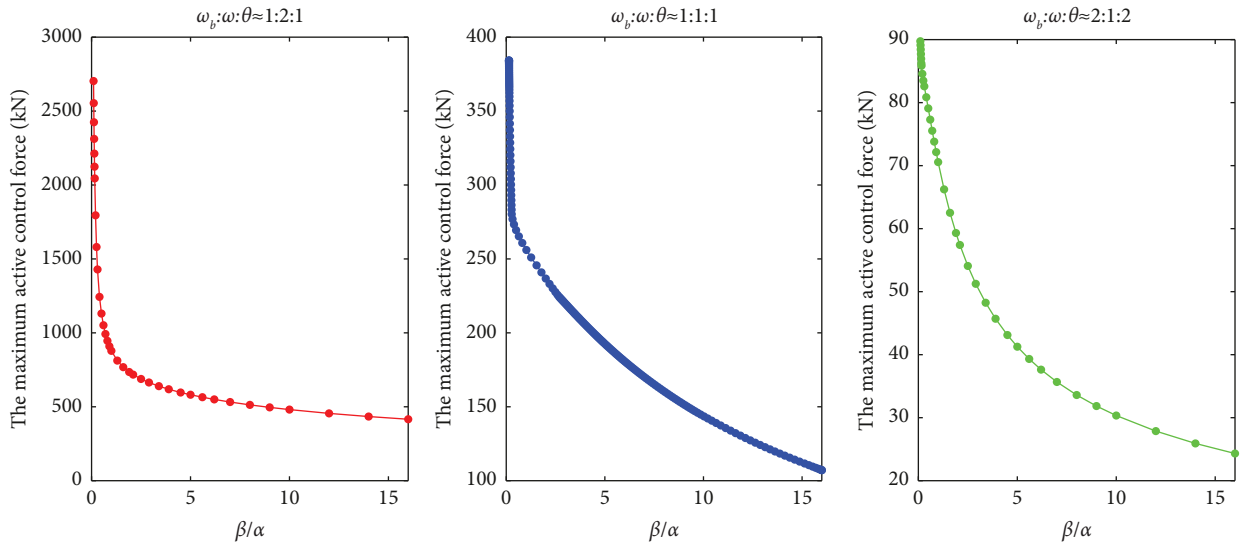


FIGURE 8: Relationship between the weight matrix coefficient ratios  $\beta/\alpha$  and maximum control force  $F_{d,max}$  of the coupled stay cable-bridge deck active control system.

design parameters with para 1, para 2, and para 3, respectively.

The fourth-order Runge–Kutta numerical analysis method was used to solve equations (29a) and (29b); for the frequency ratios  $\gamma_3$  of 1:2:1, 1:1:1, and 2:1:2, the maximum displacement responses of the stay cable at the midspan and bridge deck with the MRFD semiactive control are calculated and shown in Table 3. The semiactive control efficacy values are listed in Table 4. In addition, the relationship curves between the displacement response of the MRFD and control force were obtained and are shown in Figure 10. To give a comparison of semiactive control and widely used passive viscous control, the optimal passive control parameter, i.e., the optimal additional damping coefficient is also obtained as 577.2 kNs/m according to

equation (35) [57], and the corresponding displacement responses and control efficacies are also given in Tables 3 and 4, respectively.

$$C_{p,opt} = \frac{mL\omega}{\pi^2(l_1/L)} \cdot \frac{1}{1 - \cos a(l_2/L)}, \quad (35)$$

where  $C_{p,opt}$  is the optimal damping coefficient of the passive control and the other notations are the same as Section 2.1.

As shown in Tables 3 and 4, the MRFD semiactive control based on the branch-and-bound Hrovat optimal control algorithm achieved more significant control efficacy on cases based on the bang-bang control algorithm. Therefore, the branch-and-bound Hrovat optimal control algorithm is a better option. First, we noted that in the case of

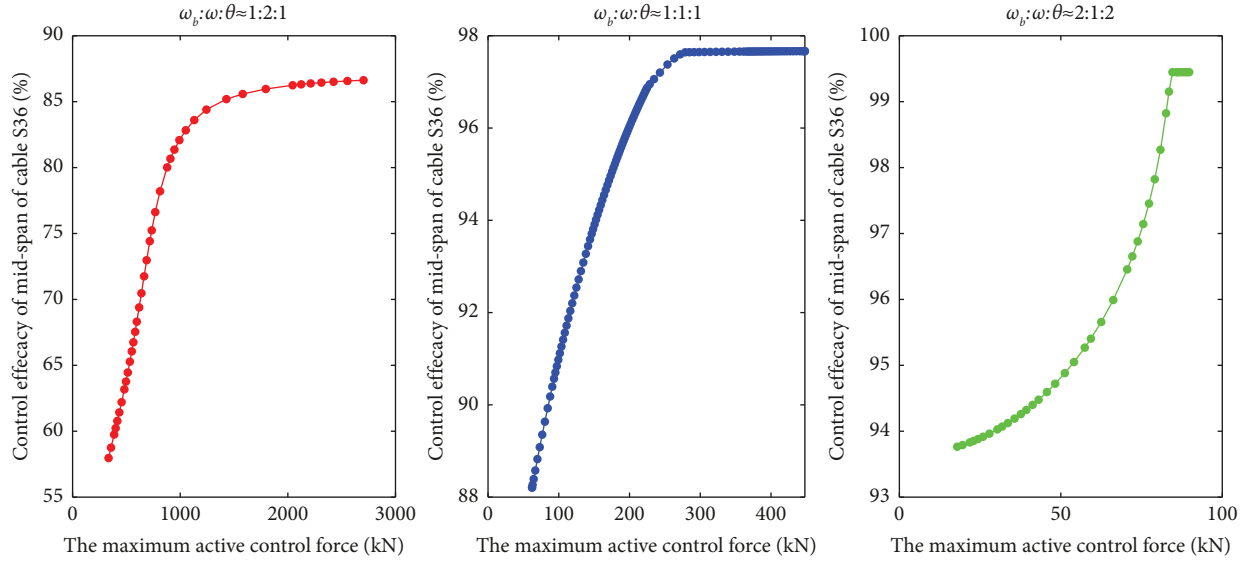


FIGURE 9: Relationship between the maximum control force  $F_{d\max}$  and control efficacies of midspan of the stay cable of the coupled stay cable-bridge deck active control system.

TABLE 2: Parameters of MRFD designed by three resonance frequency ratios corresponding to resonance.

Amplitude of design excitation	$P_0 = 80$ kN		
Optimal design weight matrix coefficient ratio	$\beta/\alpha = 1$		
$\gamma_3$ (design is based on the frequency $\gamma_3$ )	1:2:1	1:1:1	2:1:2
Name of design parameters	Para 1/Para 1-B	Para 2/Para 2-B	Para 3/Para 3-B
$ V_{a \bar{U}_{\varepsilon_d} _{\max}}(\tau) $	0.0211	0.0015	0.0017
$\bar{U}_{\varepsilon_d} _{\max}(\tau)$	7.9426	1.5704	0.7802
$\bar{s}$	8	8	8
$\bar{c}_d$	46.995	130.25	57.240
$\bar{f}_{d\max}$	6.9497	1.3741	0.6826
$U_{d\max}$ (kN)	203.21	110.91	55.100
$c_d$ (kN·s/m)	2025.0	5612.5	2466.5
$f_{d\max}$ (kN)	299.47	59.210	29.420
Maximum MRFD force for $\gamma_3 = 1: 2: 1$ (kN)	199.88	173.01	199.25
Maximum MRFD force for $\gamma_3 = 1: 1: 1$ (kN)	66.840	66.460	66.730
Maximum MRFD force for $\gamma_3 = 2: 1: 2$ (kN)	535.06	188.11	57.420

TABLE 3: Displacement response of the stay cable/bridge deck of the stay cable-bridge deck semiactive control system installed with MRFD/optimal passive control system installed with viscous damper.

$\gamma_3 = \omega_b; \omega: \theta$	Maximum displacement response at the midspan of cable (m)			Maximum displacement response at the bridge deck (m)		
	1:2:1	1:1:1	2:1:2	1:2:1	1:1:1	2:1:2
Uncontrolled	2.625	1.705	1.724	0.672	0.158	0.044
Active control	0.420	0.028	0.006	0.445	0.066	0.044
Para 1	0.358	0.031	0.443	0.317	0.061	0.044
Para 2	0.313	0.029	0.053	0.279	0.061	0.042
Para 3	0.353	0.030	0.053	0.312	0.061	0.043
Para 1-B	0.742	0.284	0.503	0.441	0.067	0.044
Para 2-B	0.874	0.212	0.061	0.472	0.062	0.044
Para 3-B	0.851	0.273	0.061	0.471	0.068	0.044
Passive control	1.223	0.373	0.049	0.538	0.062	0.044

TABLE 4: Control efficacy on the stay cable/bridge deck of the stay cable-bridge deck semiactive control system installed with MRFD/optimal passive control system installed with viscous damper.

	Control efficacy on midspan displacement response at midspan of the stay cable			Control efficacy on displacement response at the bridge deck			
	$\gamma_3 = \omega_b: \omega: \theta$	1:2:1	1:1:1	2:1:2	1:2:1	1:1:1	2:1:2
Active control		84.00%	98.34%	99.63%	33.70%	58.30%	0.24%
Para 1		89.76%	98.17%	77.31%	52.81%	61.06%	-0.46%
Para 2		88.05%	98.27%	96.87%	58.40%	60.98%	5.52%
Para 3		86.56%	98.19%	96.89%	53.52%	61.05%	3.14%
Para 1-B		71.72%	83.31%	70.83%	34.33%	57.53%	0.90%
Para 2-B		66.71%	87.57%	96.46%	29.75%	60.57%	-0.67%
Para 3-B		67.59%	83.99%	96.46%	29.87%	56.96%	0.67%
Passive control		53.43%	78.12%	97.14%	19.91%	60.44%	0.90%

resonance corresponding to  $\gamma_3 = \omega_b: \omega: \theta = 1: 2: 1$ , the MRFD designed based on the branch-and-bound Hrovat optimal control algorithm offers almost the same control efficacy for the displacement response of the stay cable at the midspan and bridge deck. In the meantime, the MRFD designed by the third set of design parameters para 3 is observed to generate the smallest MRFD force, thus para 3 is the optimal design parameter. In this scenario, the maximum MRFD force is 199.25 kN corresponding to  $\gamma_3 = \omega_b: \omega: \theta = 1: 2: 1$ , 66.73 kN corresponding to  $\gamma_3 = 1: 1: 1$ , and 57.4 kN corresponding to  $\gamma_3 = 2: 1: 2$ , respectively. In engineering practice, it is feasible to design a large-scale MRFD which is capable of generating 100~200 kN force [62, 63]. Moreover, the larger the passive viscous damping coefficient, the better the control efficacy. Comparing the active and semiactive controls in Tables 3 and 4 shows that the semiactive control efficacy was almost the same as that of the active optimal control. In some cases, the semiactive control strategy is even more effective than the active optimal control.

Table 4 shows that the semiactive control attached with MRFD could achieve better performance than the optimal active control. Figures 10(a)–10(c) show that the relationship between the displacement response and semiactive control MRFD force is consistent with that of the optimal active control when the frequency ratios  $\gamma_3 = \omega_b: \omega: \theta$  are 1: 2: 1, 1: 1: 1, and 2: 1: 2, indicating that the semiactive force of MRFD designed based on the branch-and-bound Hrovat optimal control algorithm can track and achieve the target optimal active control force. Figures 10(d)–10(f) show that the semiactive control force designed based on the bang-bang control algorithm did not track the optimal active control force much well. Moreover, the displacement-dependent negative stiffness characteristics are observed from the force-displacement trajectories in Figures 10(a)–10(c), referred to as apparent negative stiffness or pseudo-negative stiffness (PNS) [64]. The negative stiffness characteristics realized by semiactive MR damping systems are studied through numerical simulations by Li et al. [65] and demonstrated through an in situ field test of a stay cable in the Binzhou Yellow River Highway Bridge by Li et al. [50, 66]. By contrast, any passive linear viscous dampers cannot generate the control force with negative stiffness.

**3.4.2. Comparison of the Semiactive Control with the Passive Viscous Control.** The traditional passive viscous control is validated to be effective in suppressing parametric vibrations when external excitation is small [42] and is widely used in engineering practice. However, linear passive damping is not efficient enough for large-amplitude vibration [36, 67]. To give an insight into the advantage of semiactive control on large-amplitude parametric vibration, the damping effect of semiactive control and passive viscous control is evaluated and the comparison analysis is obtained.

According to equations (23b) and (35), the theoretical equivalent additional damping ratio of stay cable due to LQR-based active control can be obtained as

$$\zeta_{a,opt} = \frac{c_{p1}}{2} \cdot \sin^2(\pi(1 - \varepsilon_d)), \quad (36)$$

where  $\zeta_{a,opt}$  is the equivalent additional damping ratio of stay cable due to active control. In the study case,  $\zeta_{a,opt}$  can be calculated as 6.43%. Note that, 6.43% is not directly the additional damping ratio of the semiactive control system attached with MRFD because the practical control force of MRFD is a nonlinear hysteretic damping force. Thus, the equivalent additional damping ratio of stay cable due to MRFD can be calculated based on the principle that the dissipated energy of the nonlinear damper and the linear viscous damper is equal in per cycle under the same excitation [67–69].

Using the responses and MRFD force on the steady state of parametric resonance corresponding to the vibration frequency ratio  $\gamma_3 = \omega_b: \omega: \theta \approx 1: 1: 1$ , the hysteresis loop of MRFD under the design parameters of para 2 is obtained and shown in Figure 11. The energy dissipation per cycle equals the area of the hysteresis loop, i.e.,

$$E_d = \int_{-V_m}^{V_m} U_{\varepsilon_d|s} dV - \int_{V_m}^{-V_m} U_{\varepsilon_d|s} dV, \quad (37)$$

where  $V_m$  is the maximum damper deformation and  $U_{\varepsilon_d|s}$  is the semiactive control force of MRFD.

The equivalent additional damping ratio can be defined as

$$\zeta_{s,opt} = \frac{E_d}{4\pi E_s}, \quad (38)$$

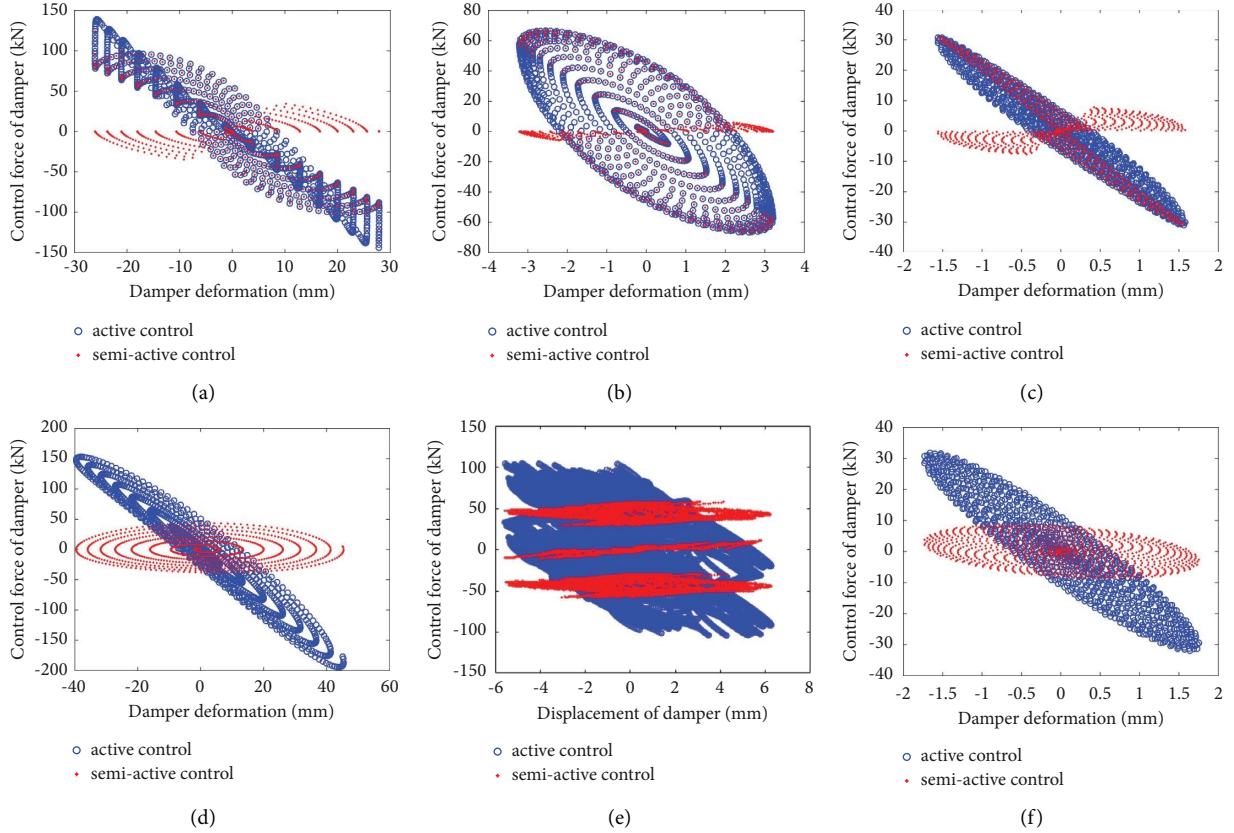


FIGURE 10: Relationship between the displacement response and the control force given by the damper: (a) frequency ratio  $[\gamma_3 = \omega]_b : \omega : \theta \approx 1:2:1$  and the parameters of MRFD are designed as para 1; (b) frequency ratio  $[\gamma_3 = \omega]_b : \omega : \theta \approx 1:1:1$  and the parameters of MRFD are designed as para 2; (c) frequency ratio  $[\gamma_3 = \omega]_b : \omega : \theta \approx 2:1:2$  and the parameters of MRFD are designed as para 3; (d) frequency ratio  $[\gamma_3 = \omega]_b : \omega : \theta \approx 1:2:1$  and the parameters of MRFD are designed as para 1-B; (e) frequency ratio  $[\gamma_3 = \omega]_b : \omega : \theta \approx 1:1:1$  and the parameters of MRFD are designed as para 2-B; (f) frequency ratio  $[\gamma_3 = \omega]_b : \omega : \theta \approx 2:1:2$  and the parameters of MRFD are designed as para 3-B.

where  $E_s$  is the elastic energy stored at the maximum displacement which can be expressed as

$$E_s = \int_0^{y_m} F_y dy(t), \quad (39)$$

where  $y_m$  is the maximum displacement of the stay cable per cycle and  $F_y$  is the approximant elastic restoring force. According to equations (29a) and (29b),  $Y(\tau) = \pi/Ly(t)$  and  $Z(\tau) = d(t)/L$ , the approximant elastic restoring force  $F_y$  can be expressed as

$$F_y = \frac{L}{\pi} y(t) + \left( \alpha_1 Lz(t) + \alpha_2 L^2 z(t)^2 \right) \frac{L}{\pi} y(t) + \alpha_3 \left( \frac{L}{\pi} \right)^2 y(t)^2 + \alpha_4 \left( \frac{L}{\pi} \right)^3 y(t)^3. \quad (40)$$

Using equations (37)–(40), the equivalent additional damping ratio  $\zeta_{s,\text{opt}}$  due to MRFD is calculated as 5.61% in the study case. It can be observed that the equivalent additional damping ratio  $\zeta_{s,\text{opt}}$  due to MRFD is slightly smaller than the theoretical equivalent additional damping ratio  $\zeta_{a,\text{opt}}$  due to LQR-based active control. This is because the nonlinear terms are neglected when designing the LQR-based controller, which is considered in the numerical simulation of the semiactive control strategy attached with MRFD.

In terms of widely used passive linear viscous control, the optimal equivalent additional damping ratio due to passive

viscous damping could be calculated as about 1.50% according to the following equation [57, 70]:

$$\frac{\zeta_{p,\text{opt}}}{\varepsilon_d} = \pi^2 \frac{C_{p,\text{opt}}}{mL\omega} \varepsilon_d, \quad (41)$$

$$\zeta_{p,\text{opt}} = \frac{x_d}{2L} = 0.5\varepsilon_d.$$

The results demonstrate that the presented semiactive control strategy attached with MRFD yields 3.74–4.27 times more additional damping than optimal passive viscous additional damping. Tables 3 and 4 also show that the



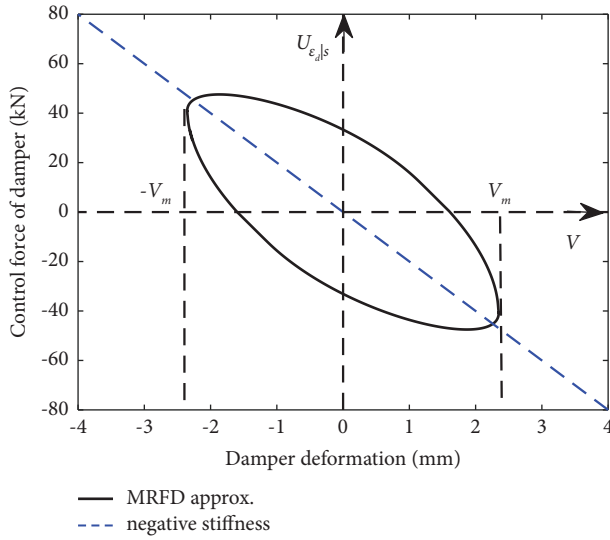


FIGURE 11: Hysteresis loop of MRFD under the design parameter para 2.

semiactive control has a much better control efficacy than the passive viscous control. Thus, the presented semiactive control strategy attached with MRFD is a promising control method since it significantly enhances the stay cable damping ratio compared to the passive oil dampers.

#### 4. Conclusions

In this study, an active control strategy based on the LQR was proposed to mitigate the parametric vibration of a super-long stay cable considering the cable-deck coupling effect. Based on the optimal active control force, a semiactive control system with negative stiffness attached with MRFD was designed to mitigate the parametric resonance of the stay cable. Two different algorithms are utilized on the semicontrol system to give a comparative analysis. A comparative analysis of semiactive control with optimal active control and passive viscous control was conducted. Parameter analysis and dynamics of active, semiactive control systems for parametric resonance of stay cable are given by numerical methods. The following conclusions can be drawn from the results:

- (1) For the frequency ratios  $\omega_b$ :  $\omega$ :  $\theta$  of approximately 1 : 2 : 1, 1 : 1 : 1, and 2 : 1 : 2, the superharmonic, primary, and main parametric resonances occur, respectively. A small excitation amplitude can arouse the large vibration for main parametric resonance, which should be paid attention to in control. When the external excitation amplitude is small, the widely used passive viscous control can effectively control the vibration of the cable. However, when it reaches a certain value, the passive viscous control cannot meet the demand for mitigating large-amplitude vibration of super-long stay cable.
- (2) The weight matrix coefficient ratio  $\beta/\alpha$  plays an important role in the proposed LQR-based active

control strategy. As the weight matrix coefficient ratio  $\beta/\alpha$  increases, the control efficacy on the midspan displacement of the stay cable first decreases sharply and then decreases slowly. The active control force also decreases with an increase in the weight matrix coefficient ratio  $\beta/\alpha$ . Both the control efficacy and force should be considered simultaneously when choosing a reasonable optimal weight matrix coefficient ratio  $\beta/\alpha$ .

- (3) The presented MRFD semiactive control can achieve the expected reduction in the response of the coupled stay cable-bridge deck system. The presented semiactive system can generate the control force with the characteristics of damping and negative stiffness, which significantly enhances the cable's damping ratio compared to the passive viscous dampers. Therefore, the semiactive control strategy attached with MRFD is expected to enable engineers to effectively mitigate the large-amplitude parametric resonance of super-long stay cables in super-span cable-stayed bridges and provide a new prospect in the relevant engineering fields.

#### Notations

$a$ :	Inclined angle of the chord from the horizontal
$A$ :	Sectional area
$\mathbf{A}$ :	Dimensionless state matrix of the system
$\mathbf{B}$ :	Dimensionless position matrix of control force
$c$ :	Damping of the stay cable
$C_b$ :	Damping of the bridge deck
$c_{p1}$ :	Dimensionless equivalent damping coefficients of the stay cable
$c_{p2}$ :	Dimensionless equivalent damping coefficients of the bridge deck
$C_{p1}$ :	Dimensionless generalised equivalent damping coefficients of the stay cable
$C_{p1}$ :	Dimensionless generalised equivalent damping coefficients of the bridge deck
$d(t)$ :	Vertical displacement of the bridge deck
$dp$ :	Dynamic arc length of the microsegment of the stay cable
$ds$ :	Microsegment initial chord length of microsegment of stay cable

$E$ :	Elastic modulus of the stay cable	$\dot{x}_d$ :	Velocity at the installation of MRFD
$f(x)$ :	Gravity sag of the stay cable	$y(t)$ :	Generalised coordinate of displacement of the stay cable from the transverse equilibrium position
$F_d(t)$ :	MR damping force	$Y(\tau)$ :	Dimensionless generalised coordinate of displacement of the stay cable from the transverse equilibrium position
$H_0$ :	Initial chordal tension of the stay cable	$Z(\tau)$ :	Dimensionless coordinate of displacement of the bridge deck
$H_d$ :	Additional chordal dynamic tension of the stay cable	$\mathbf{z}$ :	Dimensionless state vector of the system
$J$ :	Object quadratic function of the active control system	$\alpha$ :	Weight matrix coefficients of LQR controller
$K_b$ :	Stiffness of the bridge deck	$\alpha_i, i = 1, 2, \dots, 10$ :	Dimensionless coefficients in differential governing equations of the combined stay cable-bridge deck-damper active control system
$L$ :	Chord length of the stay cable	$\beta$ :	Another weight matrix coefficient of the LQR controller
$L_e$ :	Equivalent length of the stay cable	$\theta$ :	Frequency of excitation
$m$ :	Mass per unit length of the stay cable	$\omega$ :	Natural frequency of the stay cable
$M_b$ :	Mass of the bridge deck	$\omega_0$ :	Natural frequency of the standard string
$P(t)$ :	External vertical excitation directly acting on the bridge deck, $P(t) = P_0 \cos(\theta t)$	$\omega_b$ :	Natural frequency of the bridge deck
$P_0$ :	Amplitude of the excitation	$\gamma$ :	Frequency ratio of excitation to stay cable
$\mathbf{P}$ :	Symmetric positive definite matrix and solution of the algebraic Riccati equation	$\gamma_0$ :	Frequency ratio of the standard string to the stay cable
$P_{ij}, i = 1, 2, 3, 4; j = 1, 2, 3, 4$ :	Elements of $\mathbf{P}$	$\gamma_b$ :	Frequency ratio of the bridge deck to the stay cable
$\mathbf{Q}$ :	Weight matrices of the LQR controller	$\gamma_3$ :	Frequency ratio of the excitation-stay cable-bridge deck
$\mathbf{R}$ :	Another weight matrix of the LQR controller	$\lambda$ :	Proportion of the gravitational chord component to the cable's initial tension
$s$ :	Adjustable multiple	$\delta(\cdot)$ :	Unit pulse function
$R_m$ :	Mass ratio of the bridge deck block to the stay cable	$\varepsilon$ :	Dynamic strain of the microsegment of the stay cable
$T_0$ :	Initial static tangential tension of the stay cable	$\varepsilon_d$ :	Control force exerted position, $\varepsilon_d = x_d/L$
$T_d$ :	Additional tangential dynamic tension of the stay cable		
$u(x, t)$ :	Displacement from the axial equilibrium position		
$U_d$ :	Physical control force		
$\overline{U}_{\varepsilon_d}(\tau)$ :	Dimensionless generalised control force		
$v(x, t)$ :	Displacement from the transverse equilibrium position		
$x$ :	Axis coordinate		
$x_d$ :	Distance between the damper installed position and the support		

$\xi$ :	Damping ratio of the stay cable
$\xi_b$ :	Damping ratio of the bridge deck
$\tau$ :	Dimensionless time
$\dot{\bullet}, \ddot{\bullet}$ :	The first and second derivative with respect to the actual time $t$ .

## Data Availability

The data used to support the findings of the study are included within the article.

## Disclosure

*Preprint Statement.* Part of this work, specifically, Sections 2.1 and 2.2, has been preprinted ([https://assets.researchsquare.com/files/rs-3419212/v1\\_covered\\_26ddea8c-bbdf-4e3f-9fcf-52e22d8c5194.pdf?c=1697701459](https://assets.researchsquare.com/files/rs-3419212/v1_covered_26ddea8c-bbdf-4e3f-9fcf-52e22d8c5194.pdf?c=1697701459)).

## Conflicts of Interest

The authors declare that they have no conflicts of interest.

## Acknowledgments

This work was supported by the National Natural Science Foundation of China (Grant nos. 52278300, 5187849, and 51808175).

## References

- [1] K. H. Mei, Z. T. Lu, and S. J. Sun, "Property of nonlinear parametric vibration of CFRP cables," *China Journal of Highway and Transport*, vol. 20, pp. 52–57, 2007.
- [2] Q. Wu, K. Takahashi, T. Okabayashi, and S. Nakamura, "Response characteristics of local vibrations in stay cables on an existing cable-stayed bridge," *Journal of Sound and Vibration*, vol. 261, no. 3, pp. 403–420, 2003.
- [3] C. Z. Qian and C. P. Chen, "Multiple parametric resonances of taut inclined cables excited by deck vibration," *International Journal of Structural Stability and Dynamics*, vol. 18, no. 01, Article ID 1850009, 2018.
- [4] Y. B. Zhao, H. H. Lin, L. C. Chen, and C. F. Wang, "Simultaneous resonances of suspended cables subjected to primary and super-harmonic excitations in thermal environments," *International Journal of Structural Stability and Dynamics*, vol. 19, no. 12, Article ID 1950155, 2019.
- [5] G. Tagata, "Harmonically forced, finite amplitude vibration of a string," *Journal of Sound and Vibration*, vol. 51, no. 4, pp. 483–492, 1977.
- [6] J. L. Lilien and A. P. Dacosta, "Vibration amplitudes caused by parametric excitation of cable stayed structures," *Journal of Sound and Vibration*, vol. 174, no. 1, pp. 69–90, 1994.
- [7] N. C. Perkins, "Modal interactions in the non-linear response of elastic cables under parametric/external excitation," *International Journal of Non-linear Mechanics*, vol. 27, no. 2, pp. 233–250, 1992.
- [8] P. Warnitchai, Y. Fujino, and T. Susumpow, "A non-linear dynamic model for cables and its application to a cable-structure system," *Journal of Sound and Vibration*, vol. 187, no. 4, pp. 695–712, 1995.
- [9] H. M. Irvine, *Cable Structures*, MIT Press, Cambridge, MA, USA, 1981.
- [10] Y. S. Chen, *Nonlinear Vibrations*, Higher Education Press, Beijing, China, 2002.
- [11] Y. Xia and Y. Fujino, "Auto-parametric vibration of a cable-stayed-beam structure under random excitation," *Journal of Engineering Mechanics*, vol. 132, no. 3, pp. 279–286, 2006.
- [12] Z. Kang, K. S. Xu, and Z. Luo, "A numerical study on nonlinear vibration of an inclined cable coupled with the deck in cable-stayed bridges," *Journal of Vibration and Control*, vol. 18, no. 3, pp. 404–416, 2011.
- [13] J. X. Yu, J. Tian, and W. B. Dong, "Nonlinear dynamic reliability of coupled stay cables and bridge tower," *Transactions of Tianjin University*, vol. 13, pp. 334–339, 2007.
- [14] M. H. Wei, Y. Q. Xiao, H. T. Liu, and K. Lin, "Nonlinear responses of a cable-beam coupled system under parametric and external excitations," *Archive of Applied Mechanics*, vol. 84, no. 2, pp. 173–185, 2014.
- [15] L. M. Sun, L. Chen, and H. W. Huang, "Stay cable vibration mitigation: a review," *Advances in Structural Engineering*, vol. 25, no. 16, pp. 3368–3404, 2022.
- [16] B. N. Sun, Z. G. Wang, J. M. Ko, and Y. Q. Ni, "Cable parametric oscillation and its control for cable-stayed bridges," *Proceedings of SPIE- The International Society for Optical Engineering*, vol. 4330, pp. 366–376, 2001.
- [17] E. Caetano, A. Cunha, V. Gattulli, and M. Lepidi, "Cable-deck dynamic interactions at the international Guadiana bridge: on-site measurements and finite element modelling," *Structural Control and Health Monitoring*, vol. 15, no. 3, pp. 237–264, 2008.
- [18] M. Y. Liu, D. Zuo, and N. P. Jones, "Analytical and numerical study of deck-stay interaction in a cable-stayed bridge in the context of field observations," *Journal of Engineering Mechanics*, vol. 139, no. 11, pp. 1636–1652, 2013.
- [19] W. Z. Chen, Y. Zhao, and Y. Zheng, "Research for cable-girder coupled vibration of a cable-stayed bridge based on finite element analysis," in *Proceedings of the 7th International Conference on Intelligent Computation Technology and Automation*, pp. 968–971, IEEE, Changsha, China, October, 2014.
- [20] A. Javanmardi, K. Ghaedi, F. Y. Huang, M. U. Hanif, and A. Tabrizikahou, "Application of structural control systems for the cables of cable-stayed bridges: state-of-the-art and state-of-the-practice," *Archives of Computational Methods in Engineering*, vol. 29, no. 3, pp. 1611–1641, 2021.
- [21] H. Gao, H. Wang, J. Li et al., "Optimum design of viscous inerter damper targeting multi-mode vibration mitigation of stay cables," *Engineering Structures*, vol. 226, Article ID 111375, 2021.
- [22] H. Gao, H. Wang, J. Li, J. X. Mao, and Z. H. Wang, "Dynamic behavior and damping enhancement of cable with negative stiffness inerter damper," *International Journal of Mechanical Sciences*, vol. 235, Article ID 107664, 2022.
- [23] M. Liu, W. H. Yang, W. Chen, H. G. Xiao, and H. Li, "Experimental investigation on vortex-induced vibration mitigation of stay cables in long-span bridges equipped with damped crossties," *Journal of Aerospace Engineering*, vol. 32, no. 5, Article ID 04019072, 2019.
- [24] Y. F. Wang, Z. Q. Chen, C. Yang, Z. W. Liu, J. He, and Z. Q. Feng, "A novel eddy current damper system for multi-mode high-order vibration control of ultra-long stay cables," *Engineering Structures*, vol. 262, Article ID 114319, 2022.

- [25] T. Kobori, "Preface to 'Practical applications of active and semi-active structural control systems to actual civil engineering structures,'" *Earthquake Engineering and Structural Dynamics*, vol. 30, no. 11, p. 1563, 2001.
- [26] T. T. Soong and B. F. Spencer, "Supplemental energy dissipation: state-of-the-art and state-of-the-practice," *Engineering Structures*, vol. 24, no. 3, pp. 243–259, 2002.
- [27] F. Casciati and M. Domaneschi, "Semi-active electro-inductive devices: characterization and modelling," *Journal of Vibration and Control*, vol. 13, no. 6, pp. 815–838, 2007.
- [28] Y. Ikeda, "Active and semi-active vibration control of buildings in Japan—practical applications and verification," *Structural Control and Health Monitoring*, vol. 16, no. 7–8, pp. 703–723, 2009.
- [29] M. Domaneschi, "Feasible control solutions of the ASCE benchmark cable-stayed bridge," *Structural Control and Health Monitoring*, vol. 17, pp. 675–693, 2009.
- [30] M. Domaneschi and L. Martinelli, "Performance comparison of passive control schemes for the numerically improved ASCE cable-stayed bridge model," *Earthquakes and Structures*, vol. 3, no. 2, pp. 181–201, 2012.
- [31] M. Domaneschi, "Simulation of controlled hysteresis by the semi-active Bouc-Wen model," *Computers and Structures*, vol. 106–107, pp. 245–257, 2012.
- [32] M. Domaneschi and L. Martinelli, "Optimal passive and semi-active control of a wind excited suspension bridge," *Structure and Infrastructure Engineering*, vol. 9, no. 3, pp. 242–259, 2013.
- [33] X. C. Zhang, X. Zhang, Y. X. Zhao, J. Zhao, and Z. D. Xu, "Experimental and numerical studies on a composite MR damper considering magnetic saturation effect," *Engineering Structures*, vol. 132, pp. 576–585, 2017.
- [34] D. Pisanski, "Optimal control of structures subjected to traveling load," *Journal of Vibration and Control*, vol. 24, no. 7, pp. 1283–1299, 2018.
- [35] W. X. Wang, Z. L. Yang, R. K. Hu, X. G. Hua, and X. Y. Wang, "Active tendon control of stay cable by a giant Magnetostrictive actuator considering time-delay," *Applied Sciences*, vol. 12, no. 5, p. 2666, 2022.
- [36] X. Shi, S. Y. Zhu, and S. Nagarajaiah, "Performance comparison between passive negative-stiffness dampers and active control in cable vibration mitigation," *Journal of Bridge Engineering*, vol. 22, no. 9, Article ID 04017054, 2017.
- [37] J. P. Ou and H. Li, "Design approaches for active, semi-active and passive control systems based on analysis of characteristics of active control force," *Earthquake Engineering and Engineering Vibration*, vol. 8, no. 4, pp. 493–506, 2009.
- [38] S. Y. Ok, D. S. Kim, K. S. Park, and H. M. Koh, "Semi-active fuzzy control of cable-stayed bridges using magnetorheological dampers," *Engineering Structures*, vol. 29, no. 5, pp. 776–788, 2007.
- [39] D. A. Shook, P. N. Roschke, and O. E. Ozbulut, "Superelastic semi-active damping of a base-isolated structure," *Structural Control and Health Monitoring*, vol. 15, no. 5, pp. 746–768, 2008.
- [40] A. Bahar, F. Pozo, L. Acho, J. Rodellar, and A. H. Barbat, "Hierarchical semi-active control of base-isolated structures using a new inverse model of magnetorheological dampers," *Computers and Structures*, vol. 88, no. 7–8, pp. 483–496, 2010.
- [41] S. Laflamme, D. Taylor, M. Abdellaoui Maane, and J. J. Connor, "Modified friction device for control of large-scale systems," *Structural Control and Health Monitoring*, vol. 19, no. 4, pp. 548–564, 2012.
- [42] C. B. Xiong, L. Y. Yu, L. Abi, and Z. H. Lu, "Step-control and vibration characteristics of a hybrid vehicle suspension system considering energy consumption," *Vehicle System Dynamics*, vol. 60, no. 5, pp. 1531–1554, 2022.
- [43] A. Rodriguez, N. Iwata, F. Ikhoulane, and J. Rodellar, "Model identification of a large-scale magnetorheological fluid damper," *Smart Materials and Structures*, vol. 18, no. 1, Article ID 015010, 2009.
- [44] K. Hiramoto, T. Matsuoka, and K. Sunakoda, "Semi-active vibration control for approximating the targeted active control output," in *Proceedings of the 2013 Proceedings of SICE Annual Conference (SICE)*, pp. 929–934, Nagoya, Japan, September, 2013.
- [45] S. G. Liu, L. F. Feng, D. Zhao et al., "The development of an outer multi-pole magneto-rheological damper with high dynamic range of damping force," *Smart Materials and Structures*, vol. 27, no. 11, Article ID 115025, 16 pages, 2018.
- [46] Y. F. Duan, Y. Q. Ni, and J. M. Ko, "Cable vibration control using magnetorheological dampers," *Journal of Intelligent Material Systems and Structures*, vol. 17, no. 4, pp. 321–325, 2006.
- [47] X. Shi and S. Y. Zhu, "Magnetic negative stiffness dampers," *Smart Materials and Structures*, vol. 24, no. 7, Article ID 072002, 2015.
- [48] R. L. Jiang, X. T. Rui, M. Wei, F. F. Yang, H. T. Zhu, and L. L. Gu, "A phenomenological model of magnetorheological damper considering fluid deficiency," *Journal of Sound and Vibration*, vol. 562, Article ID 117851, 2023.
- [49] W. X. Wang, X. G. Hua, X. Y. Wang, J. L. Wu, H. X. Sun, and G. B. Song, "Mechanical behavior of magnetorheological dampers after long-term operation in a cable vibration control system," *Structural Control and Health Monitoring*, vol. 26, no. 1, Article ID e2280, 2019.
- [50] H. Li, M. Liu, J. H. Li, X. C. Guan, and J. P. Ou, "Field tests of vibration control of stay cables by using magnetorheological fluid dampers," in *Proceedings of the 2005 IEEE International Symposium on Intelligent Control & 13th Mediterranean Conference on Control and Automation*, Limassol, Cyprus, June, 2005.
- [51] W. J. Wu and C. S. Cai, "Cable vibration control with a semiactive MR damper-numerical simulation and experimental verification," *Structural Engineering and Mechanics*, vol. 34, no. 5, pp. 611–623, 2010.
- [52] Q. Zhou, S. R. K. Nielsen, and W. L. Qu, "Semi-active control of three-dimensional vibrations of an inclined sag cable with magnetorheological dampers," *Journal of Sound and Vibration*, vol. 296, no. 1–2, pp. 1–22, 2006.
- [53] Q. Zhou, S. R. K. Nielsen, and W. L. Qu, "Semi-active control of shallow cables with magnetorheological dampers under harmonic axial support motion," *Journal of Sound and Vibration*, vol. 311, no. 3–5, pp. 683–706, 2008.
- [54] M. Liu, V. Sethi, G. B. Song, and H. Li, "Investigation of locking force for stay cable vibration control using magnetorheological fluid damper," *Journal of Vibration and Acoustics*, vol. 130, no. 5, Article ID 054504, 2008.
- [55] H. W. Huang, L. M. Sun, and X. L. Jiang, "Vibration mitigation of stay cable using optimally tuned MR damper," *Smart Structures and Systems*, vol. 9, no. 1, pp. 35–53, 2012.
- [56] L. F. Zheng, *Stability and Dynamic Performance Analysis of Parametric Vibration of Stay cable in cable-stayed Bridge with Super-long Span*, Harbin Institute of Technology, Harbin, China, 2018.
- [57] R. Q. Long, *Research on Dynamic Characteristics and Design Method of Parametric Vibration Control System for Super Long*

- Stay Cables*, Harbin Institute of Technology, Harbin, China, 2019.
- [58] M. Liu, L. F. Zheng, P. Zhou, and H. G. Xiao, "Stability and dynamics analysis of in-plane parametric vibration of stay cables in a cable-stayed bridge with superlong spans subjected to axial excitation," *Journal of Aerospace Engineering*, vol. 33, no. 1, Article ID 04019106, 2020.
- [59] S. M. Zheng, Q. Shen, C. Guan, H. G. Cheng, H. Zhuang, and M. Zhou, "Semi-active control of seismic response on prestressed concrete continuous girder bridges with corrugated steel webs," *Applied Sciences*, vol. 12, no. 24, Article ID 12881, 2022.
- [60] T. T. Soong and B. F. Spencer, "Active structural control: Theory and practice," *Journal of Engineering Mechanics*, vol. 118, no. 6, pp. 1282–1285, 1992.
- [61] R. Stanway, J. L. Sproston, and N. G. Stevens, "Non-linear modelling of an electro-rheological vibration damper," *Journal of Electrostatics*, vol. 20, no. 2, pp. 167–184, 1987.
- [62] G. Yang, B. F. Spencer, J. D. Carlson, and M. K. Sain, "Large-scale MR fluid dampers: modeling and dynamic performance considerations," *Engineering Structures*, vol. 24, no. 3, pp. 309–323, 2002.
- [63] G. Yang, B. F. Spencer, H. J. Jung, and J. D. Carlson, "Dynamic modeling of large-scale magnetorheological damper systems for civil engineering applications," *Journal of Engineering Mechanics*, vol. 130, no. 9, pp. 1107–1114, 2004.
- [64] L. Chen, L. M. Sun, and S. Nagarajaiah, "Cable with discrete negative stiffness device and viscous damper, Passive realization and general characteristics," *Smart Structures and Systems*, vol. 15, no. 3, pp. 627–643, 2015.
- [65] H. Li, M. Liu, and J. P. Ou, "Negative stiffness characteristics of active and semi-active control systems for stay cables," *Structural Control and Health Monitoring*, vol. 15, no. 2, pp. 120–142, 2008.
- [66] J. P. Ou and H. Li, "Analysis of capability for semi-active or passive damping systems to achieve the performance of active control systems," *Structural Control and Health Monitoring*, vol. 17, no. 7, pp. 778–794, 2010.
- [67] E. Rosenblueth and I. Herrera, "On a kind of hysteretic damping," *Journal of the Engineering Mechanics Division*, vol. 90, no. 4, pp. 37–48, 1964.
- [68] Z. Zhang, M. Q. Niu, K. Yuan, and Y. W. Zhang, "Research on linear/nonlinear viscous damping and hysteretic damping in nonlinear vibration isolation systems," *Applied Mathematics and Mechanics*, vol. 41, no. 7, pp. 983–998, 2020.
- [69] H. M. Dwairi, M. J. Kowalsky, and J. M. Nau, "Equivalent damping in support of direct displacement-based design," *Journal of Earthquake Engineering*, vol. 11, no. 4, pp. 512–530, 2007.
- [70] B. M. Pacheco, Y. Fujino, and A. Sulekh, "Estimation curve for modal damping in stay cables with viscous damper," *Journal of Structural Engineering*, vol. 119, no. 6, pp. 1961–1979, 1993.